UNIVERSITAT POLITÈCNICA DE CATALUNYA
BARCELONATECH
Escola Superior d'Enginyeries Industrial,
Aeroespacial i Audiovisual de Terrassa

Degree: Master's Degree in Aerospace Engineering

Student: Campos Murcia, Daniel

STUDY: 3D MODELING AND INITIAL STRUCTURAL ANALYSIS OF A LIGHT AIRCRAFT

REPORT

Director: Vives, David

Codirector: Roca, Xavier

Delivery date: 20-06-2019

Call: Spring Year 2018

ACKNOWLEDGMENTS

Voldria dedicar aquests treball de final de màster al senyor Marc Kuster, qui ha compartit la seva passió i el seu projecte personal amb mi, per tal de poder elaborar un treball en base a un cas d'aplicació real.

Aquest treball també va dedicat als meus germans i amics per la infinita paciència que han demostrat a l'aguantar-me en els moments de màxim estrès.

Voldria agrair també a l'equip docent de l'ESEAIAAT l'acompanyament rebut durant la meva etapa formativa, i en especial al professor David Vives per tutoritzar aquest projecte.

Finalment m'agradaria agrair el projecte a la Marta Reales Moreno, que durant els sis anys d'etapa universitària ha sigut el motor que m'ha fet seguir en els moments més difícils. Qui ha hagut de suportar hores i hores de converses infinites sobre avions i qui, en última instància, m'ha ajudat a desenvolupar aquest projecte.

Sense vosaltres res d'això hagués sigut possible. Moltes gràcies a totes i tots.

Daniel Campos Murcia

ABSTRACT

En un país on l'aviació es vista com un problema i no com una solució, pocs són els afortunats i valents per ser partícips d'aquest meravellós sector. Dins d'aquests pocs, hi ha persones com en Marc Kuster que van més enllà del simple fet de volar, i porten la seva afició fins al punt de dissenyar i construir els seus propis avions.

Aquesta tesi s'emmarca dins del projecte personal d'en Marc Kuster, qui fa més de 20 anys va dissenyar un avió de tres superfícies amb la intenció de que algun dia fos realitat.

L'ODYSSEUS II, és el producte d'aquest somni, i en aquesta tesis es mostren parts del seu procés de disseny i anàlisis de l'avió. EN concret, l'estudi es basa en el desenvolupament dels diferents models CAD i els primers anàlisis i estudis en el camp aerodinàmic, estructural i de comportament.

In a country where aviation is seen as a problem and not a solution, few are the lucky and brave to be part of this wonderful sector. Among these few, there are people like Marc Kuster who go beyond the simple fact of fly, and take their hobby to the point of designing and building aircraft.

This thesis is part of the personal project of Marc Kuster, who more than 20 years ago designed a three-surface airplane with the intention that one day it would become a reality.

The ODYSSEUS II, is the product of that design, and in this thesis parts of the airplane design and analysis process are shown. In particular, the thesis is based on the development of the different CAD models and later some first studies are made on the structural, aerodynamic and performance behaviour of the airplane.

LIST OF CONTENTS

Aim ..... Page 1

Justification ..... Page 2

Scope ..... Page 3

Requirements ..... Page 4

1. State of the Art ..... Page 6

1.1 Experimental Amateur-Built Aircraft ..... Page 6

1.2 Structure Construction Technologies ..... Page 8

1.3 Materials in Sport Aviation ..... Page 14

2. Thesis and Design Methodologies ..... Page 18

2.1 Design Phases ..... Page 18

2.2 Thesis Methodologies ..... Page 20

3. CAD Models ..... Page 21

3.1 Aerodynamic Model ..... Page 23

3.2 Structural Model ..... Page 24

3.3 Conceptual Model ..... Page 26

4. Aerodynamic Studies ..... Page 35

4.1 Studies Methodology ..... Page 36

4.2 Three Surface Aircraft Particularities ..... Page 37

4.3 Airfoil Selection ..... Page 39

4.4 Aircraft Aerodynamics' Preliminary Evaluation ..... Page 40

4.5 Computational Fluid Dynamics ..... Page 48

5. Structural Studies ..... Page 56

5.1 Flight Envelope ..... Page 57

5.2 Structural Pre-Sizing ..... Page 61

5.3 Finite Element Analysis ..... Page 70

6. Performance Studies ..... Page 78
6.1 Weight and Balance ..... Page 78
6.2 Range Estimation ..... Page 87

7. Conclusions ..... Page 89
7.1 Aerodynamic Conclusions ..... Page 89
7.2 Structural Conclusions ..... Page 89
7.3 Performance Conclusions ..... Page 90
7.4 Thesis Conclusions ..... Page 91
7.5 Future Work ..... Page 91

8. References ..... Page 92

9. Budget ..... Page 94

10. Annexes ..... Page 95

LIST OF FIGURES

Figure 1. Original sketches of ODYSSEUS II ..... Page 5
Figure 2. Bending Stress Diagram ..... Page 9
Figure 3. Truss-Type Structure ..... Page 11
Figure 4. Semi-monocoque Structure ..... Page 11
Figure 5. Monocoque Structure ..... Page 12
Figure 6. Typical Wing Structure ..... Page 13
Figure 7. Typical Wood Sections ..... Page 14
Figure 8. Typical Metal Wing Spars ..... Page 16
Figure 9. Preliminary Design Diagram ..... Page 20
Figure 10. CAD Model for CFD ..... Page 23
Figure 11. Wing Shell Model ..... Page 25
Figure 12. Tail Shell Model ..... Page 25
Figure 13. ODYSSEUS II ..... Page 27
Figure 14. Internal Airframe ..... Page 28
Figure 15. Wing Box ..... Page 28
Figure 16. Glider Wing Attaching System ..... Page 29
Figure 17. Wing Structure ..... Page 30
Figure 18. Tail Structure ..... Page 31
Figure 19. Landing Gear ..... Page 32
Figure 20. ODYSSEUS II Exterior ..... Page 33
Figure 21. ODYSSEUS II Interior ..... Page 33
Figure 22. ODYSSEUS II panel ..... Page 34
Figure 23 CG positioning comparison ..... Page 38
Figure 24. Wing design ..... Page 41
Figure 25. Canard Design ..... Page 41
Figure 26. Tail Surface Design ..... Page 42
Figure 27. Full Aircraft Designed in XFLR5 ..... Page 43
Figure 28. Example of mass distribution ..... Page 44
Figure 29. CL-alpha Curve ..... Page 45
Figure 30. Polar Curve ..... Page 45
Figure 31 Aerodynamic Efficiency Curve ..... Page 46
Figure 32. Cm-alpha Curve ..... Page 47
Figure 33. Cl versus speed Curve ..... Page 48
Figure 34. Ansys 17 Mesh ..... Page 49
Figure 35. CFD Aerodynamic Coefficients ..... Page 51
Figure 36. CFD polar Curve ..... Page 52

Figure 37. CFD Aerodynamic Efficiency ..... Page 52
Figure 38. CFD Drag vs Speed ..... Page 53
Figure 39. Stall Speed Studies ..... Page 55
Figure 40. ODYSSEUS II Flight Envelope ..... Page 61
Figure 41. Wing Section Idealization ..... Page 62
Figure 42. Wing Loads Idealization ..... Page 62
Figure 43. Idealized lift distribution ..... Page 64
Figure 44. Main Wing Pre-sizing Results ..... Page 67
Figure 45. Composite Analysis Scales ..... Page 70
Figure 46. Main Wing Mesh ..... Page 73
Figure 47. Wing Boundary Conditions ..... Page 74
Figure 48. Von Misses stress over skin ..... Page 75
Figure 49. Von Misses Stress over the internal str. ..... Page 75
Figure 50. Wing Displacements ..... Page 75
Figure 51. Tail Mesh and Boundary Conditions ..... Page 76
Figure 52. Von Misses Stress over Tail ..... Page 77
Figure 53. Aircraft Reference System ..... Page 78
Figure 54. CG-Envelope ..... Page 86
Figure 55. Payload-Range Diagram ..... Page 88
Figure 56. ODYSSEUS II Range over Europe ..... Page 88

LIST OF TABLES

Table 1. Airfoil Characteristics ..... Page 39
Table 2. Moment Coefficient and Trimming ..... Page 47
Table 3. Canard CFD Parameters ..... Page 50
Table 4. Flight Envelope parameters ..... Page 57
Table 5. Main Wing Pre-sizing ..... Page 65
Table 6. Materials' Mechanical Properties ..... Page 65
Table 7. Main Wing Sizing results ..... Page 66
Table 8. Front Wing Pre-sizing parameters ..... Page 68
Table 9. Front Wing Sizing results ..... Page 68
Table 10. Tail Pre-sizing Parameters ..... Page 68
Table 11. Tail Sizing results ..... Page 69
Table 12. Homogenized Material's properties ..... Page 72
Table 13. Weight Estimation inputs ..... Page 79
Table 14. Aircraft Weights and CG ..... Page 81
Table 15. Aircraft Wight items ..... Page 82
Table 16. Loading Cases ..... Page 83
Table 17. Loading Cases ..... Page 87
Table 18. Hiring Fees ..... Page 94
Table 19. Study Development Detailes ..... Page 94
Table 20. Software and Licences ..... Page 94

AIM

The aim of this thesis is to develop a 3D model of the airplane designed by Marc Kuster in the 90's and to carry out some preliminary analyses to evaluate the aerodynamic behaviour of same.

The second objective is to develop a structural design of this airplane, followed by a first iteration in analysis using "Finite Element Analysis" software.

JUSTIFICATION

The thesis presented in this report is included within the conceptual design framework of the ODYSSEUS II aircraft designed by Marc Kuster.

The conceptual design phase is absolutely necessary when designing an aircraft and if the intention is to finish building it.

In amateur construction, calculations and construction processes are usually not as strict as it is in conventional construction. This can pose a safety problem for the future operation of the aircraft, and more if the aircraft is made of composite materials.

The thesis that is presented provides calculations and analysis necessary to evaluate the behavior and safety of the aircraft and thus help the designer with the new design and calculation methodologies, so he can continue with his project.

SCOPE

This project encompasses the following aspects.

- Study of plans and requirements delivered by the client.
- Examinations of the following:
    - Amateur construction.
    - Types of aeronautical structures.
    - Type of materials used in amateur aircraft construction.
- Development of a 3D model compatible with CFD software.
- Elaboration of a 3D model compatible with FEM software.
- Development of a conceptual 3D model that allows the obtention of the dimensions and weights of the different components.
- Aerodynamic study based on the customer's original design including:
    - The elaboration of model and calculations by means of potential theory.
    - The preparation of a CFD study for this airplane.
- Structural study based on the most critical flight conditions including:
    - Flight envelope study.
    - Preliminary calculations.
    - Analysis through FEM.
- Study of the general behaviour of the aircraft including:
    - CG-Envelope diagram
    - Stability study
    - Range study

This project is not intended to be a complete development of the aircraft design. For reasons of time, the thesis presented here is a preliminary document of the basics, which will allow one to carry out further designs and calculations refinements, leading ultimately to a final blue print.

REQUIREMENTS

This thesis offers technological support to the engineer and home builder Marc Kuster in his quest to design and build a 3 surfaces plane based on composite materials.

The basic parameters, as suggested by Mr. Kuster are as follows.

So, the customer's requirements are

- Category : Standard Light Aircraft, (max. 5000 lbs)
- Nominated cruise speed : 170 kts
- Max. speed : 220 kts
- VNE : 250 kts
- MTOW : 1170 kg
- Minimum range, w/o reserve : 6.5 hours[1]
- Climb rate @MTOW : 1200 fpm AMSL
- Take off distance @MTOW : 550 m AMSL
- Landing distance @MTOW : 400 m AMSL
- Max stall speed (clean) : 52 kts
- Max seats : 4
- Number of engine : 1
- Cabin pressurization : Nil
- Limits : + 6G / -3G
- Composite Structure
- The 3D models developed throughout the study must comply with the geometrical restrictions present in the plans developed by the client and which can be seen in Figure 1.

For any other issue, CS23 and FAR23 standards are taken as reference, although this aircraft is classified in the Experimental Catergory (Non Type Certified Aircraft).

[1] Range based on the Lycoming IO-390 engine.

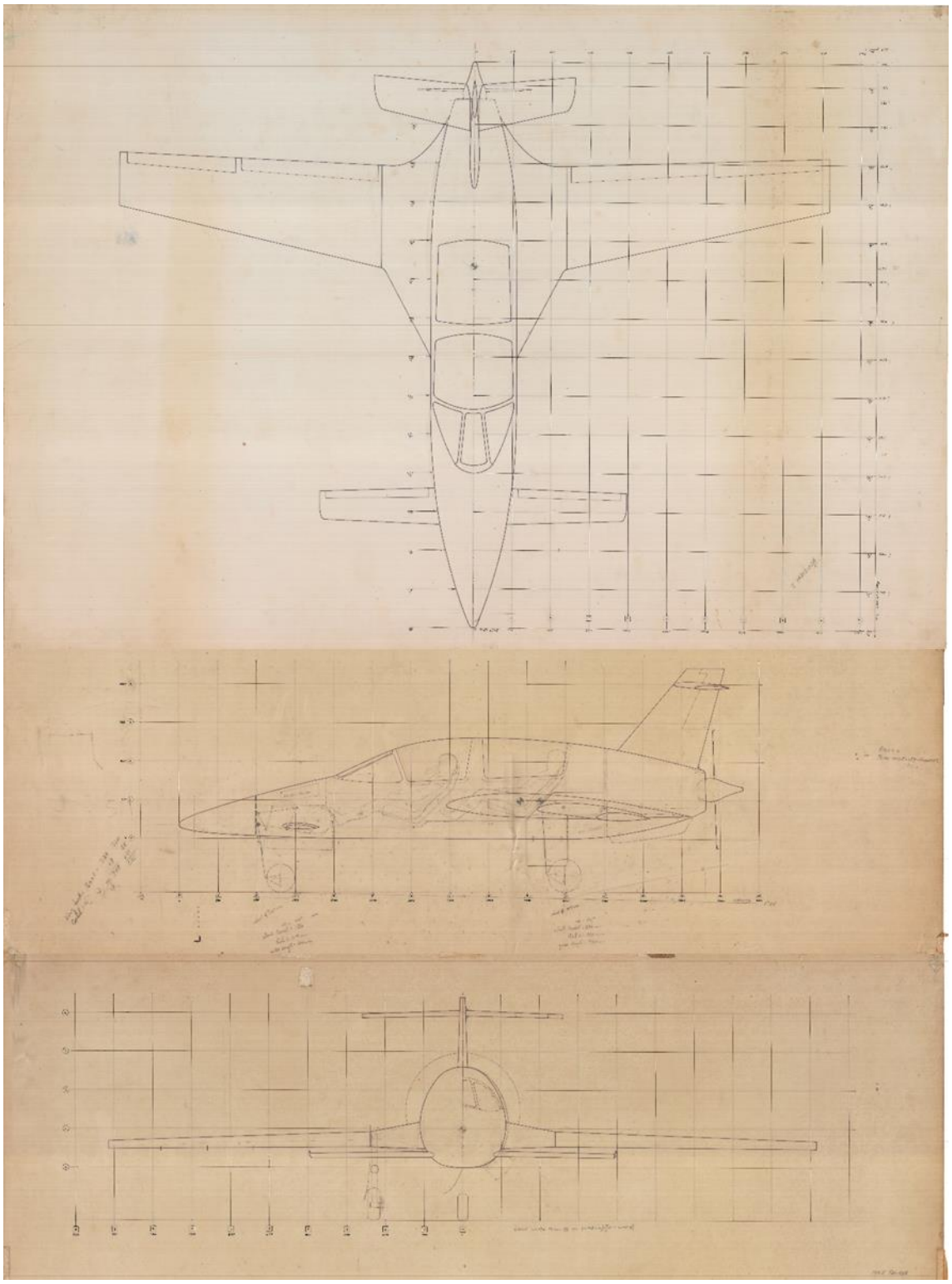

Figure 1. Original sketches of ODYSSEUS II aircraft designed by Marc Kuster.

1. STATE OF THE ART

1.1 EXPERIMENTAL AMATEUR-BUILT AIRCRAFT

Experimental amateur-built aviation, also known as homebuilts, is a growing activity within the world of sports aviation. The basic idea is that the enthusiast builds his own aircraft.

The most common forms of constructions are: Own Design, Plan Built or Kit Built constructions. Restorations of old aircrafts also have a strong following in many countries around the world.

The Homebuilder's main aim is to enjoy the construction and finally flying his own creation.

Although, a priori this type of undertaking would suggest an increased level of danger, it soon becomes evident that through adherence to strict aeronautical engineering practices, quality controls and legislations regulating these activities; those potential dangers are reduced to exceptionally low levels.

The most substantial number of followers are in the United States, where tens of thousands of people and many associations dedicate their effort and free time to this wonderful pastime, with the Experimental Aircraft Association (EAA) having the highest membership, country and worldwide. Other countries with large groups of homebuilders are: Australia, New Zealand and South Africa.

Within Europe, there are countries with a strong aeronautical culture the likes of France, Germany, the UK, Czech Republic and Slovenia.

France has the distinction of being the world's first country to promote "Homebuilding", started in 1934.

In most other countries of Europe, there is a steady growth of experimental aircraft construction with Spain being no exception.

Questions which are often asked in the general aviation circles are: "Why are these types of aircraft becoming more and more popular?".

According to the article available in reference [1], it often can be simply the challenge. The immensely rewarding experience of having created such a project with one's own hand is emotionally important to many people.

Aviation is expensive and for many an aspiring aviator, the costs of a factory built, certified aircraft are prohibitive. The expensive upkeep and maintenance costs are often a deterrent too.

With homebuilts, the construction costs are essentially carried by the buildery. Certified components often cost astronomical sums of money due to insurance premiums. A large portion of these costs are not applicable in the homebuilt sector.

Uniqueness is another consideration. It is fair to say that no homebuilt is the same. The freedom to choose paint, instrumentation, upholstery, in some cases engines and much more, are all plus points for the individualist. The completion of such an undertaking ends up being a reflection of the person who built such an aircraft.

In addition, the fact of having this freedom, allows the builder to use the latest technological advances which are not always available on certified machines. The results often translate into better performances and higher efficiencies.

Another interesting aspect of Homebuilding is the fact that a large inventory of second hand components is available worldwide making acquisitions more cost effective.

Such components are not so easily available in the certified aircraft sector, due to for example the "Time Ex" factor, meaning that such components may have reached the end of its hourly or cycle life.

A final point on the subject of economics, the possibility of being able to carry out the maintenance and some inspections, also saves substantial amounts of costs.

Homebuilding has some down sides. To build an aircraft is not for everyone and the investment in large quantities of materials and tooling may cause some people to think twice before undertaking such a venture. Also, for many folks, manual work is foreign to them.

The essence of owning an experimental aircraft is meant for leisure activity. For those who wish to use a homebuilt aircraft as a business tool, the current regulations restrict such activities in many countries. Flying a homebuilt fore hire and reward, i.e. commercial activity, is prohibited.

Experimental Aviation (the word "experimental" being somewhat a misnomer) is a world that has brought aviation closer to many people who could not otherwise have had access to flying.

In this thesis, the reader may find some of the analyses and procedures helpful to build an experimental aircraft.

1.2 STRUCTURE CONSTRUCTION TECHNOLOGIES

When faced with any problems, mankind has for eons developed and evolved methods and solutions to overcome them.

In the case of aircraft manufacturing, and specifically airframe manufacturing, the development of fabrication methodologies has been tightly linked with aerodynamic and materials advances.

In this section, a brief summary of the different types of existing structures, their pros and cons, following the references [2], [3] and [4] is put forward.

1.2.1 Aircraft Loads

Before investigating the structural topic, the main loads an aircraft is subjected to in flight are presented herein. Such loads are to a large extent the criteria used to decide which structure will best apply.

During the flight of any aircraft, there are 3 types of loads to which the structure of the aircraft must face:

- Aerodynamic Loads: The aerodynamic loads are generated by the pressure differences created on the aircraft during the flight. This pressure differences are responsible for generating the forces of lift and drag, and moments, causing bending and torsion in the wing among other elements. Generally, these forces depend on the geometry of the aircraft, its weight and the flight conditions.
- Inertial Loads: Inertial loads are those forces and moments generated by aircraft accelerations generally due to the variation of G forces during flight.
- Operational Loads: Are those loads that are given by the use of the plane, such as those due to the pilot climbing the wing to enter the cabin.

As a general rule, the dimensioning of the structure is based on the first two types of forces, focusing mainly on the aerodynamic loads.

With regards to the reaction of the structure to the aforementioned loads, there are five main stresses appearing:

- Tension: This type of stress appears when trying to separate an element through the application of a traction effort in its axial component.
- Compression: The compression is the stress opposite to the tension, appearing this when an effort of crushing is applied on the longitudinal axis of the component.
- Torsion: This type of stress appears when a force or moment of twist is applied on the element.
- Shear: This type of stress appears when the material is opposed to a layer of material sliding on its attached layer.
- Bending: It appears when compression and traction efforts are combined. It generates a curvature on the piece to which said efforts are applied.

During the flight of an airplane, all the above mentioned reactions are possible to appear. The tension and compression are present on the wings due to the lift and drag forces through their combined form, the bending. The torsion appears as a result of the different moments in flight, whether they are aerodynamic or inertial. Union elements, such as screws and pins, are subjected to high shear forces.

Figure 2 shows a diagram that shows the different types of stress that appear in a plate type element, such as for example the skin of the wing or the fuselage.

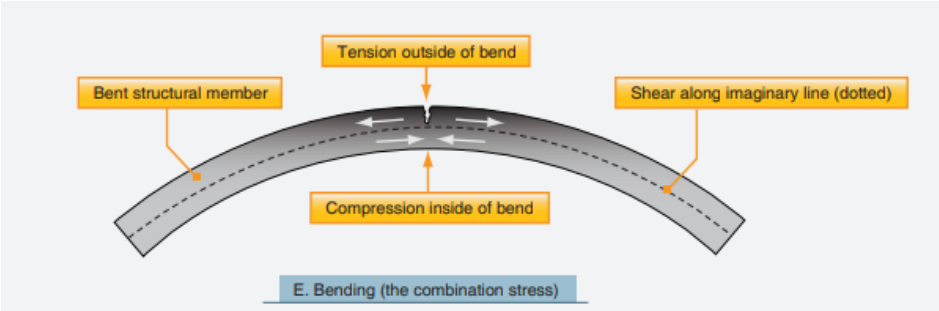

Figure 2. Bending Stress Diagram. Extracted from [3]

1.2.2 Aircraft Structures

With the knowledge of the types of loads the structure of this aircraft is subjected to, the author of the thesis has looked at the different types of structures available.

Each of these types has advantages and disadvantages, and are in some cases the result of the evolution of a previous type of structure due to the application of the latest technologies and materials.

Fuselage

The fuselage is the body of the plane. In it, not only are located the crew and the passage, but also the space for storing different systems and joining the different components which allow the aircraft to fly.

Historically, Truss-type fuselages were the first to appear. At the beginning, manufactured in wood and later in metal, they constitute a framework based on the union of rigid elements such as tubes or struts resisting the different loads. Many times, this type of structure is accompanied by tensioners which contribute with an extra resistance against tensile loads. These type of structures are complex to design, have a fairly good weight resistance ratio, although the number of elements is high and there is a sensitivity to buckling present. Trust construction is still used today on some occasions, but is somewhat a thing of the past.

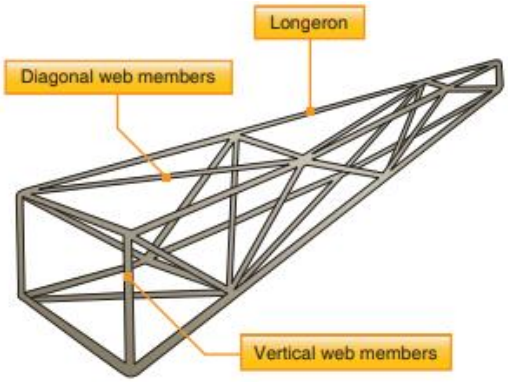

Figure 3. Truss-Type Structure. Extracted from [3]

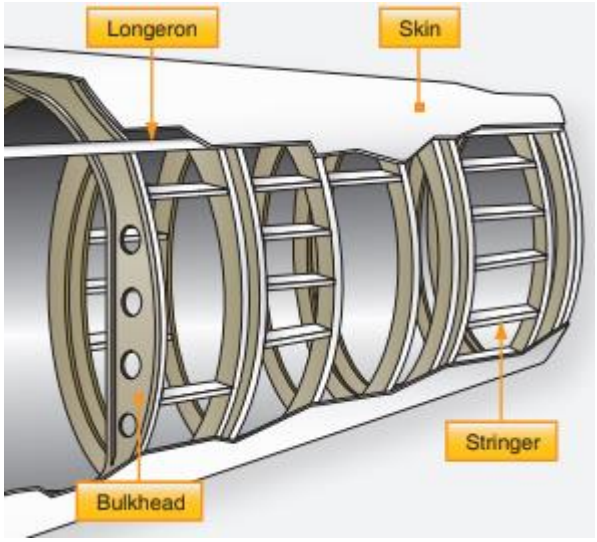

Figure 4. Semi-monocoque Structure. Extracted from [3]

The next type of structure is the semi-monocoque. This type of structure combines frames and stringers with structural skin. While the first elements are responsible for resisting the various loads and being the support for the skin, the skin is responsible for providing structural stiffness, keeping the different elements together. In turn, the skin also provides the aerodynamic finish necessary to reduce aerodynamic drag. This type of structures present a lower complexity when it comes to being designed and a better behavior against buckling with a smaller number of pieces. The lightness of semi-monocoque is similar to that of the truss structure.

A variant of the semi-monocoque structures.

In them the stringers and longerons are eliminated thanks to a better design and resistance of the skins. In these structures, the skin takes on a larger structural role since it is responsible for supporting the different types of loads.

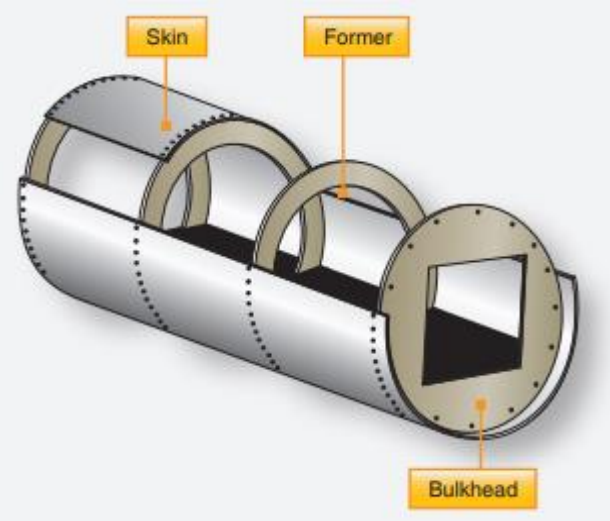

Figure 5. Monocoque Structure. Extracted from [3]

As a result, the application of this type of structures produces lighter airframes than semi-monocoque constructions. The down side is a slightly reduced resistance against buckling.

Wings and Empennage

Wings and tail surfaces are the components of an aircraft subjected to the highest efforts and stresses, as they are responsible for generating the lift which counteracts the weight of such a machine. The unwelcomed by-product of these efforts and stresses is called Drag.

It is interesting to note that the type of wing structures of has not changed much over time. The same components are still used today as those produced more than 50 years ago. A testimony to the ingenuity of the designers of times go by.

The technological advances lie in the use of new materials and the number of elements which form the structure of the wing. A good example of such improvements is the number of wing ribs a sports plane requires, often less than ten per half wing, compared to up to thirty some 50 years ago.

Flying surfaces, whether wings or tails, are composed of three main components: the spars, the ribs and the skin.

Spars are the main structural components of a wing. They are in charge of sustaining bending and torsion efforts. Generally, and depending on the type of aircraft, the number of spars is usually 2, sometimes 3.

Some of the newer models of ultralight aircraft contain only 1 spar per half wing, thanks to the advances made in terms of composite elements.

Ribs are the components responsible for the shape of the aerodynamic profile of a wing. They are also responsible for transmitting the aerodynamic loads towards the beam.

The number of ribs in a wing depends on the type of skin of a wing, the greater the resistance to buckling of the skin, the fewer ribs needed.

The third and last component is the skin, which is responsible for producing the aerodynamic finish required for flight efficiency. The skin, as an integral part of the structure is used to reinforce the resistance against wing twist and forms a type of torsion box together with the two spars.

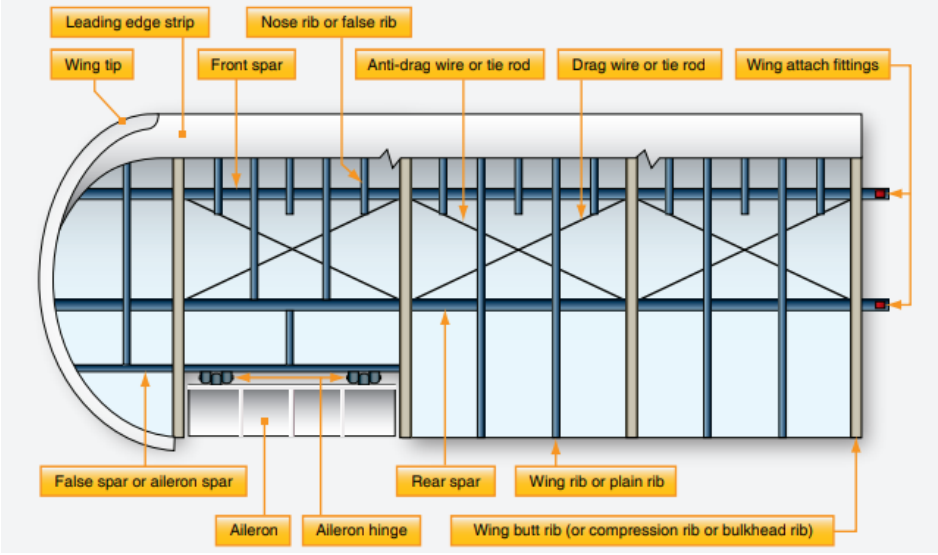

Figure 6. Typical Wing Structure. Extracted from [3]

1.3 MATERIALS IN SPORT AVIATION

Relating to the previous section, brief comparison of the different materials often used when manufacturing an aircraft and in this case an experimental one, is herewith presented.

1.3.1 Wood

At the beginning of aviation, only wood was used in the structural construction of the aircraft. And for the most pioneering, wood had to be natural.

The advantages offered by this material is the availability, the low cost, the little requirement of specialized tools and that it is easy to work given the few construction skills.

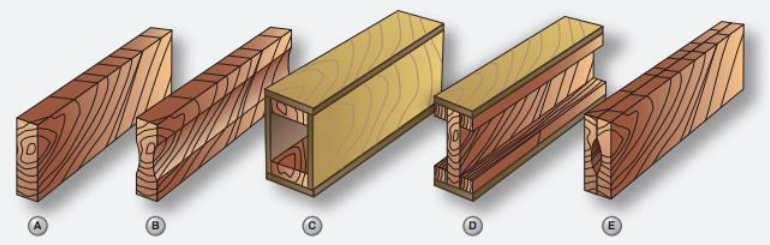

Figure 7. Typical Wood Sections. Extracted from [3]

1.3.2 Aluminum Alloys

Relatively early in the history of aviation, aluminium constructions started to appear. Different alloys were tried.

The advantages of aluminium alloys are: a good strength to weight ration as proven through many laboratory tests, a relatively good resistance to corrosion, as well as a good resistance to temperature variations.

The price of aluminum alloys, compared to composite materials, is lower. In addition, the handling and machining of aluminium is simple and strait forward. Sheet metal work experience is required to obtain suitable forms.

Also, of interest is the fact that aluminium is an isotropic material. It offers a high versatility in many applications, regardless of grain orientation, which is not the case with steel, for example.

Finally, the components are much easier to evaluate compared to other materials, so the maintenance cost of the aircraft is lower. Is a great material for home-builders.

A notable and substantial weakness of aluminum is the fact that it does not have a defined fatigue limit. This means that in the case of dynamic loads, a component may fail with low loads, if the number of cycles is high enough.

In addition, aluminium, when subjected to fatigue has a much lower tensile strength compared to its normal maximum resistance to the traction. This consideration implies that components have to be produced with a larger quantity of metal in order to overcome this problem. And more material equals more weight. It also implies that the total weight is greater than a structure that only faces static charges.

Another problem with aluminium is corrosion. Several types of corrosion rear their ugly heads. Inter granular corrosion occurs in aluminium alloys especially 2024T3, which has copper as its main alloying component, when subjected to water condensation and or high atmospheric humidity contents causing aluminium oxide, a white powdery substance.

Stress corrosion forms fissures between in the homogeneity of the aluminum degrading and weakening the area until rupture in some cases. The causes of stress corrosion are vibration and excessive tension, compression, torsion, shear and bending loads.

Finally, aluminium has a great predisposition to galvanic corrosion. This occurs when two metals with different electrical properties come into contact. Due to the difference in electric potential, an electrical current is generated between the two metals causing said corrosion.

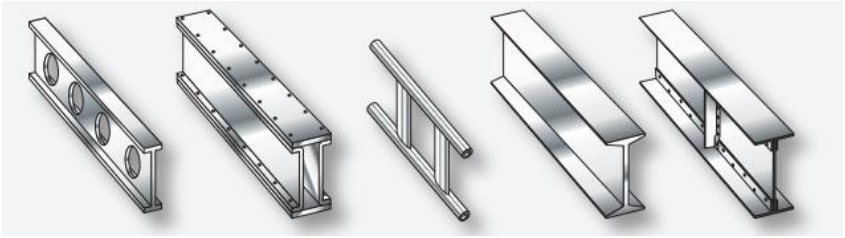

Figure 8. Typical Metal Wing Spars. Extracted from [3]

1.3.3 Composite Materials

The combination of two or more compounds with completely different properties in order to form a new material with remarkably better features, offers the opportunity to manufacture components with greater resistance and lower weight. Lighter, faster and more resistant aircraft construction results in better performance and lower fuel/energy consumption.

Thus, composite materials stand out for their high strength, light weight, flexibility, and the ease of building complex compound curves, which are difficult to produce with aluminum. They also have a high dielectric strength, good dimensional stability and no corrosion issues.

Unfortunately there are disadvantages with composites as well. Toxicity of the resins, some sensitivity to impacts, limited resin and catalyst storage times, potential mixing ratio issues and ambient working temperatures are a few.

A high degree of vigilance is required when working especially with epoxy resins, all of it adding to the final price tag.

As with all materials, composite constructions required some specific protection from the elements. To minimize heat absorption on surfaces exposed to the sun, it is recommended to use light colors, the lighter the better. White being the least heat absorbent.

Lightning strikes can cause serious damages to structures and auxiliary components in a composite aircraft and it is of the utmost importance to channel these very high electric charges in a safe manner.

Aluminum aircrafts are essentially Faraday cages and therefor mostly impervious to lightening, whereas composites aircrafts are not.

Aluminum is still the predominant material with experimental aircrafts, but composites are slowly catching up, despite the more complex manufacturing processes and associated costs.

The legendary aircraft engineer and designer Burt Rutan set the pace of composite aircraft constructions as early as the 1970's.

2. THESIS AND DESIGN METHODOLOGIES

As mentioned in previous sections, the objective of the Project is to analyze the aerodynamics of the ODYSSEUS II aircraft and use the results to design a structure of composite materials, which will then be briefly analyzed. This type of Project is included in the preliminary design phase.

For the benefit of the reader, a prior knowledge is helpful to better understand the context of thesis. To do so, the Standard Methodology of aircraft design is explained below. For more information, the reader can consult references [2], [4], [7] and [8].

2.1 DESIGN PHASES

In engineering, the development of a product is not a trivial procedure, but a drawn out and detailed process, often feedback-type and only complete when the objectives and criteria of service meet all the requirements imposed.

In the aeronautical sector, this design process is somewhat more complex due to the high demands imposed on an aircraft and the various tests and evaluations to which the design must be submitted.

As a general rule, the steps one must follow in order to design and build an aircraft are:

1. **Requirements Definition:** In this first stage the designer and the client meet to define the different requirements that the plane must fulfil. In this step it is also important to record the type of certification you want to obtain.
2. **Conceptual Design**: The second step is to brainstorm and market research to have one or several positions with which to solve the problem raised in the requirements stage.
3. **Preliminary Design**: This stage is one of the most extensive of the process, since it is about defining, studying and carrying out the first calculations and simulations based on the design or closed designs in the conceptual phase. Within the preliminary design, it is crucial to study the aerodynamics, the flight mechanics, the structures and the stability of the aircraft.
4. **Detail Design**: Once the simulations and preliminary calculations indicate that the design meets the requirements set, each of the aircraft's components is designed and tested and the necessary documentation is generated to manufacture it.
5. **Flight test**: With the first prototype built, different flight tests are carried out to verify the calculations made.
6. **Critical Design Review**: This stage of the design process is critical, since it evaluates the results obtained and redesigns those components that may pose some type of problem for the proper functioning of the aircraft.
7. **Certification**: With the closed, tested and verified design, the certification of the aircraft is carried out.

The afore mentioned points are not a linear process, but a recursive process where the aim is to optimize the concept initiated in the conceptual design phase, until obtaining the best possible solution.

2.2 THESIS METHODOLOGIES

This thesis is included in the framework of preliminary design phase of the ODYSSEUS II aircraft designed by Marc Kuster. The methodology used is described in the diagram of Figure 9 and is based on the realization of a CAD model necessary to carry out the different preliminary studies of the aircraft.

Once finished, aircraft's aerodynamic are studied and the designed structure is simulated by means of FEM.

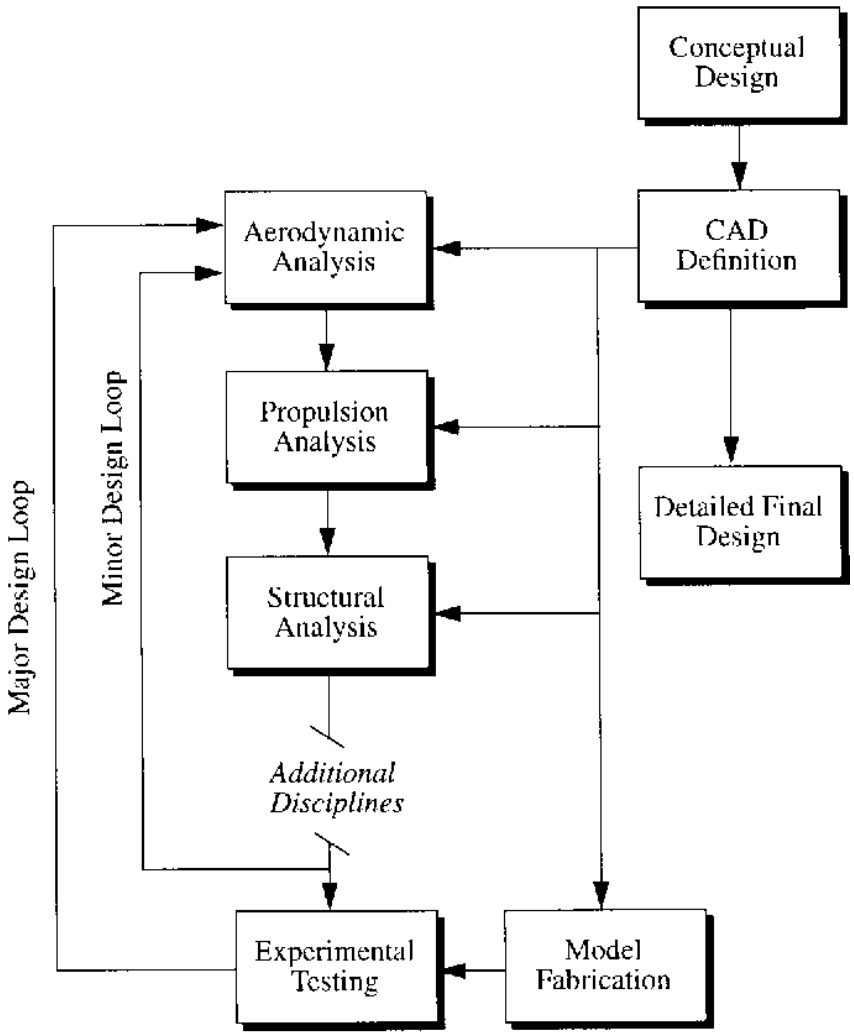

Figure 9. Preliminary Design Diagram. Extracte from [9]

3. CAD MODELS

In order to carry out these studies, several characteristic models of the aircraft are required in order to interact with different specific software within each of the areas subject to study.

In this way, the author of the project has developed three different models meeting the different needs and requirements to carry out studies concerning the aerodynamics, the structural calculation and the visualization of the entire product.

These models have been developed through the use of CATIA V5 R2017. Catia is a software of parametric design widely used in the engineering industry and especially used for the aeronautical sector.

This software offers a great variety of modules and complements that allow to carry out specific tasks according to the work sector of the person who is in charge the design.

As it is indicated on its website (reference [5]),

> *CATIA, which is based on the 3DEXPERIENCE platform of Dassault Systèmes, offers the following:*
>
> *Social design environment based on a unique source of authenticity, accessed through powerful 3D panels that drive business intelligence, simultaneous real-time design and collaboration of all stakeholders, including mobile workers.*
>
> *3DEXPERIENCE offers an intuitive experience with top-level 3D modeling and simulation functionalities that optimize the efficiency of all experienced and sporadic users.*
>
> *It is an inclusive product development platform, which is easy to integrate with existing processes and tools. This allows several disciplines to take advantage of effective and integrated specialized applications in all phases of the product development process.*

The author of the thesis has decided to use this software due to the experience he has in the use of this tool, since he has not only used this program for personal and academic projects but also is a frequent tool in his work environment.

The recurring modules to carry out the project shown in this document are:

- Part Design,
- Assembly Design,
- Generative Shape Design
- Drafting.

These modules, frequently in the aeronautical sector, have a specific and unique function that, by combining them in an adequate way, are capable of realizing anything that one can imagine.

The module of Part Design is the most basic of CATIA. In it, the designs of the different pieces and components is used to carry out the design of different sections such as fuselage frame, wing ribs, etc.

The Assembly Design module is used to join the different parts created and that make up an assembly or set of parts with a purpose. This module also allows evaluating design features such as assembly weight, center of gravity, inertia, etc.

This is very useful when making predictions and using these parameters to carry out simulations and calculations. With the Assembly Design module, it is not only possible to assemble parts, but it is also possible to compose assemblies with bases to sub-assemblies. A good example of this module is the subsequent assembly of wings, canard, fuselage and tail which then become the entire aircraft.

The GSD module is a tool requiring advanced knowledge of the program. This module is used to design the surfaces and any element, usually finished components, but with "visible" internal parts.

In the aeronautical and composite materials sector, it is an essential module since its power is used to transform into reality the different aerodynamic profiles and characteristic shapes of an aircraft. In addition, in the field of composite materials, this module is used to carry out the Shell type models (see section 5.3) used in the different calculation and simulation software.

Finally, the Drafting module is used to generate drawings, both of the components and of the final assembly.

3.1 AERODYNAMIC MODEL

The aerodynamic model is used to carry out the various simulations using Computational Fluid Dynamics.

This model traces the exterior geometry of the airplane and simplifying those elements of small size which may disturb the continuity of the surface and compound errors in the mesh and, therefore, in the final calculation of the aerodynamic loads. Thus, elements such as holes, antennas and complex geometries have been removed or simplified to develop this model.

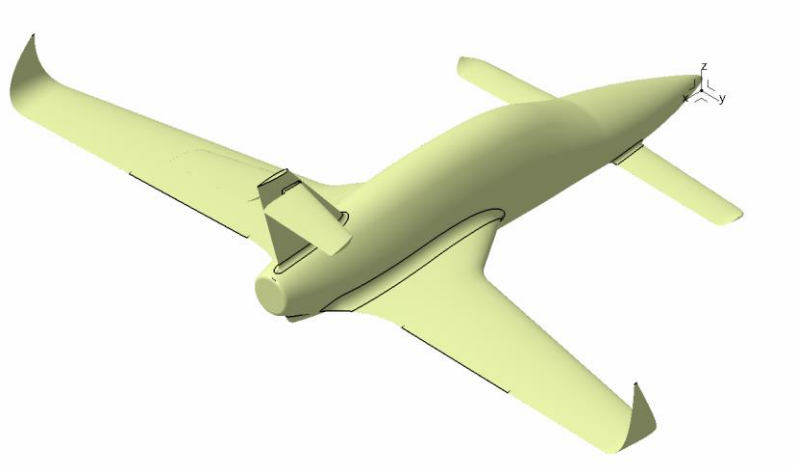

Figure 10. CAD Model develope in order to perform CFD simulations

As seen in Figure 7, the aerodynamic model has all lines smoothed out between the different elements making up the aircraft. In addition, this model is a faithful reproduction of the original design seen in Figure 1, except for the winglets added by the author of the thesis, which have being acknowledged and accepted by the designer. These winglets have been inserted in order to improve the aerodynamic characteristics of the airplane.

The model is made in 1:1 scale and has been exported in *.stp* format to carry out the meshing in any of the different software existing in the market.

3.2 STRUCTURAL MODEL

The structural model can be very different depending on the type of structure of the aircraft and the type of analysis that is needed to perform it. Concerning this thesis, the complete structure of ODYSSEUS II is based on a monocoque structure made entirely of composite materials, combining carbon fiber, Kevlar and fiberglass. This particular structure makes this model necessary in order to calculate the structural behavior required of a Shell type. The study of the structure proposed for the ODYSSEUS II is carried out through the evaluation of the macro-scale material or component scale. This means that the strength of the material is evaluated according to the type of composite material layerings.

The shell type models are based on the creation of the outer or inner surface of the component manufactured from laminar materials (such as composites). They are used as a reference in the calculation software, which determines the layers to be evaluated. Based on said surface, section 5.3 explains more about this type of analysis.

In this case study, the model of the complete structure of the aircraft has been developed. However, only wing and tail structural models have been used to perform the analysis. The particularity of this type of model lies in the use of the surfaces as a reference of the real structural elements, without taking into account the real thickness of the components.

As shown in Figures 11 and 12 the level of sizes is much higher than the aerodynamic model. Furthermore, it can be seen that the design of components is based on surfaces and not on solids, as mentioned above. In the two proposed models, details such as fuel tanks and or ailerons can be noted. These elements are not taken into account during the structural analysis, as these are focused on in the behavior of the main structures of the assemblies.

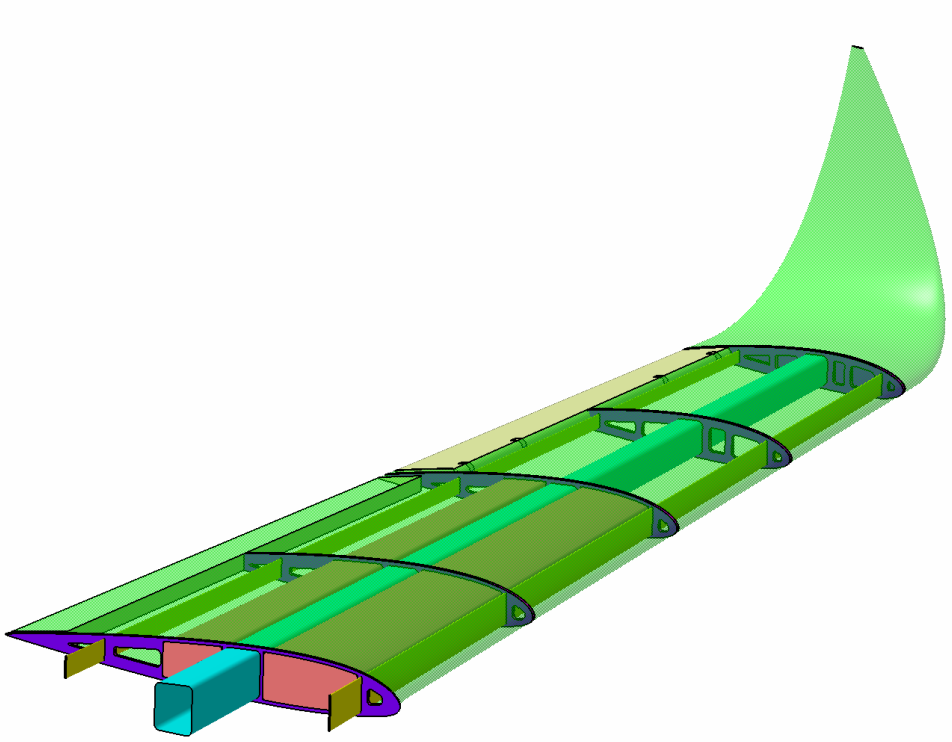

Figure 11. Wing Shell Model

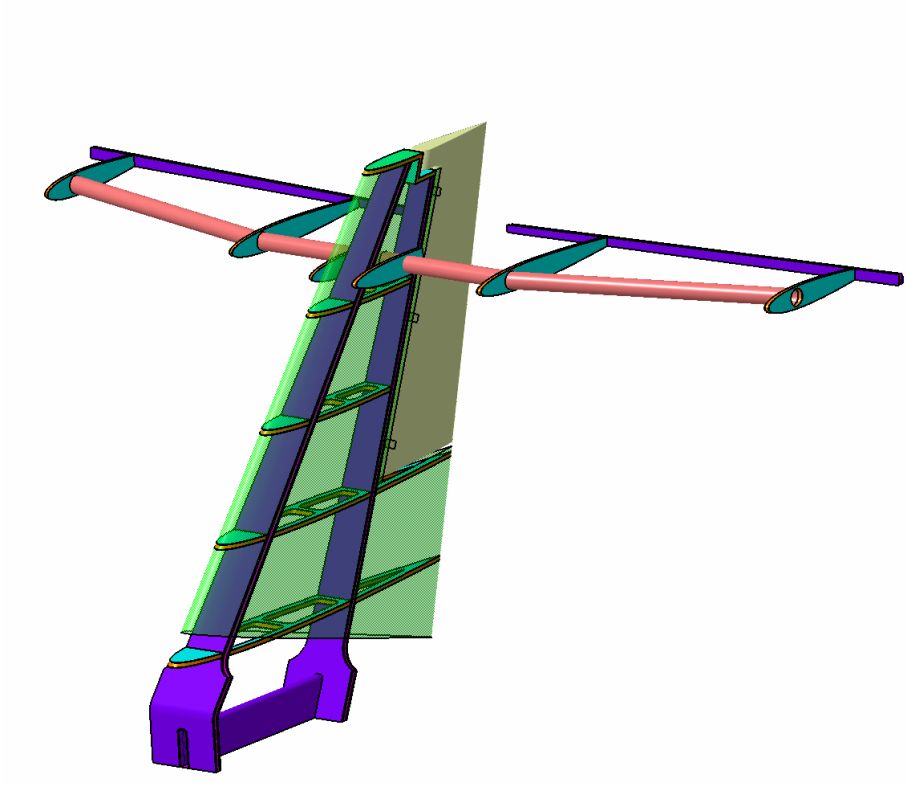

Figure 12. Tail Shell Model

3.3 CONCEPTUAL MODEL

The last model that has been developed within the framework of this thesis is the conceptual model. This last model is the most detailed since the different parts and components of the aircraft have been modeled in greater detail to obtain the first estimates of the dimensioning of the parts, as well as to calculate the total weight of the structural and the center of gravity.

In turn, this model helps to have a clearer vision of what the aircraft is like and allows to evaluate factors that are not as relevant as the aerodynamics of the aircraft or its structure, but that take on some importance when manufacturing the aircraft as they can be the positioning of the different systems, the ergonomics and comfort of the passengers, the accesses to carry out the maintenance, etc.

Below is a list of renders created by the KEYSHOT 6 program based on the conceptual model designed in CATIA V5.

As mentioned in section 3.2, the design of the ODYSSEUS II structure is based on a structure of monocoque type where both the interior structure and the skin are used to support the different structural loads. In this way it has been defined that the base material of the internal structure is the carbon fiber, either in combination with foam to generate panels or substructures type sandwich.

Figure 13 shows a general view of the exterior of the aircraft, consisting mainly of glass fiber with the different carbon fiber control surfaces. The reality is, that the skin of the fuselage is made of glass fiber because the level of load that it must withstand is very inferior to the one of the wings or other elements.

With regard to wings, tail and canard, the skin is composed of a stack that combines both the glass fiber and carbon fiber, being the outer layer made of glass fiber.

Figure 13. ODYSSEUS II

With regards to the internal structure of the ODYSSEUS II, it is necessary to differentiate the various elements making up the complete structure.

In the airframe of the fuselage, it can be noted how the different bulkheads and formers uniformly distribute the loads and are responsible for providing structural rigidity to the skin, this by transmitting said loads to both the upper and lower longitudinal reinforcements.

The lower reinforcements also form a structural core, which is responsible for supporting the floor of the cabin, withstand the impacts of the landing gear and to dampen the efforts and stresses transmitted from the wing to the wing box.

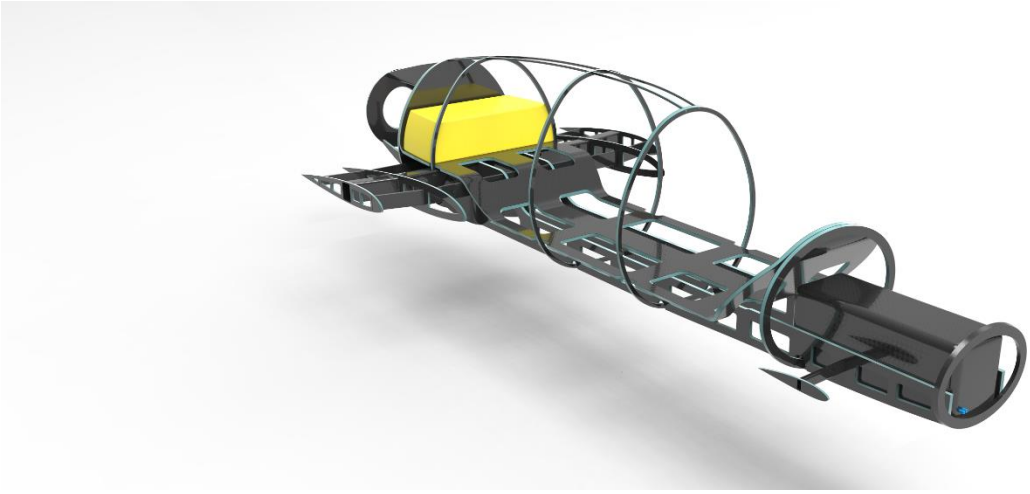

Figure 14. Internal Airframe

The wing box has been designed to support the wing loads and the main landing gear. In addition, it allows the rapid disassembly of the wings in the event of road transport.

As shown below, three hollow spars allow the accommodation of the main spar and the stringers of the wing that are attached by a pin, a common practice in glider construction.

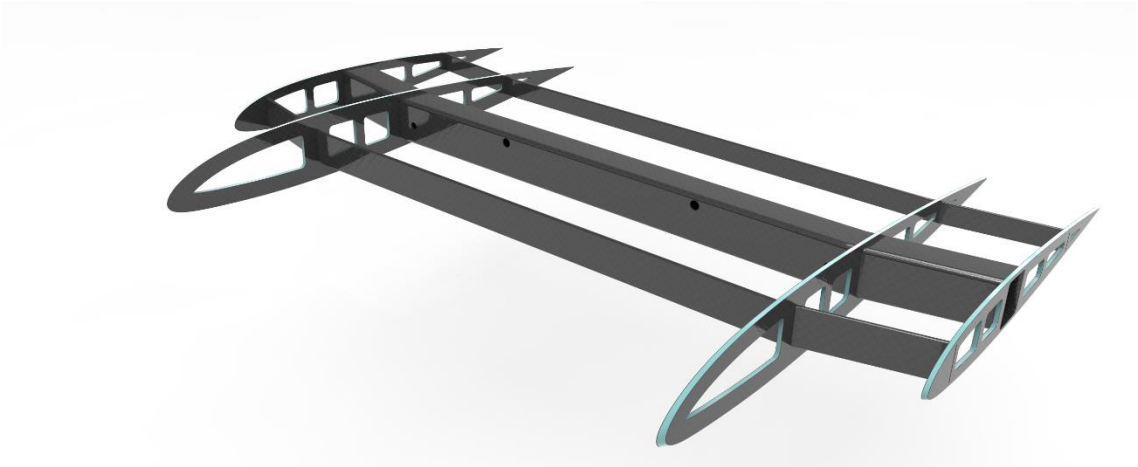

Figure 15. Wing Box

Figure 16. Glider Wing Attaching System. Extracted from [6]

The structure of the wing is based on a central beam/main spar located around 40% of the chord of the wing.

The main spar is the principal load carrier and also responsible for supporting the bending stresses together with the help of two secondary spars. These secondary spars close up the torsion box, together with the skin of the upper and the lower wing profile. This concept is responsible for minimizing torsional stresses. The hinges of the ailerons and the simple flap mechanism are mounted on the rear spar.

Finally, winglets, ailerons and flaps are based on a core foam construction, reinforced by a spar (in the case of aileron and flap tube) and covered by a carbon fiber skin. This mode of construction widely used in the field of amateur aviation allows one to obtain light structures with high resistance, both to the aerodynamic loads and against impact.

The few ribs present on the ODYSEUS II wings are used as support to the skin, avoiding any deformation of the leading edges due to compressive loads.

Finally, the wing has two integrated fuel tanks that are shown in yellow in the Figure 17.

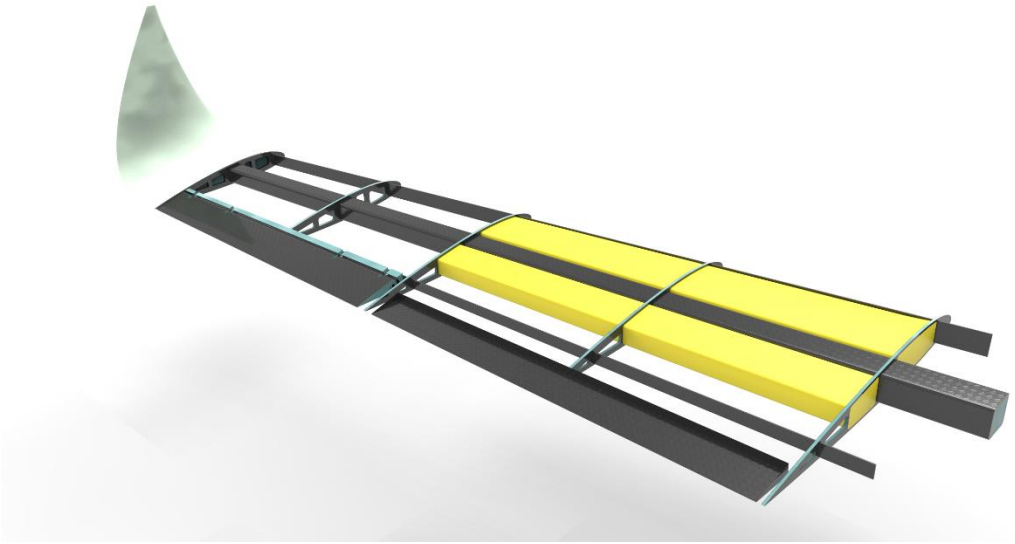

Figure 17. Wing Structure

The philosophy used in the design of the tail is conceptually identical to the rest of the structure. Therefore, an internal structure based on carbon ribs with foam core, form the resistant center of the tail. In turn, the carbon fiber skin provides extra resistance against torsional loads.

As shown in Figure 18, the horizontal empennage is composed entirely of a foam core reinforced with a front tubular spar, a rear spar and two ribs on each side. This type of empennage, used as the elevator is a full flying wing and the most important element in the maneuver of an aircraft in pitch axis.

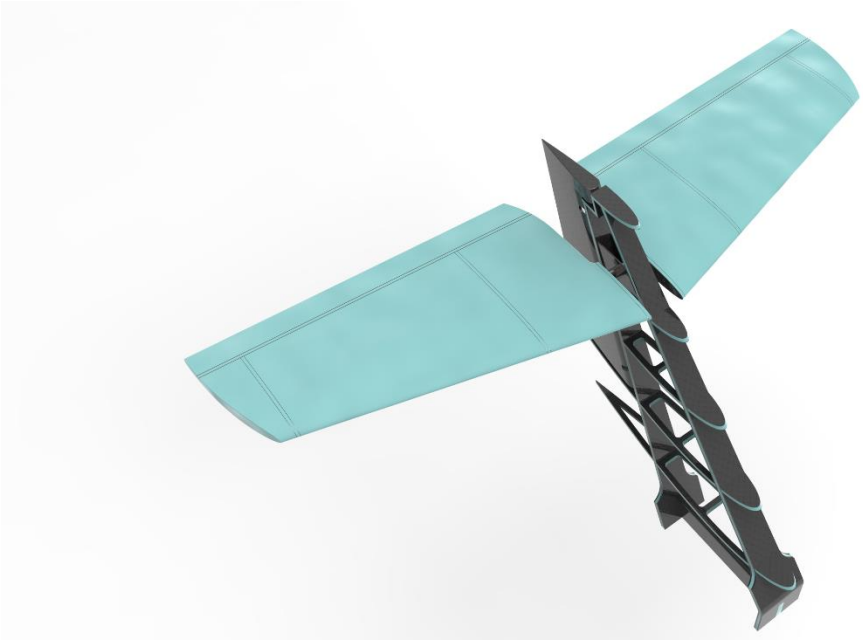

Figure 18. Tail Structure

The tricycle-type landing gear is fully integrated into the fuselage structure and wing box of the ODYSSEUS II. In this way it is possible to disassemble the wings to carry out any repair, modification or transport.

This is an important feature, in that the fuselage is fully supported on the undercarriage assembly, even with the wings removed.

As can be seen, the main landing gear transmits the loads towards the central beam of the wing box, while the nose gear rests directly on the longitudinal reinforcements of the fuselage.

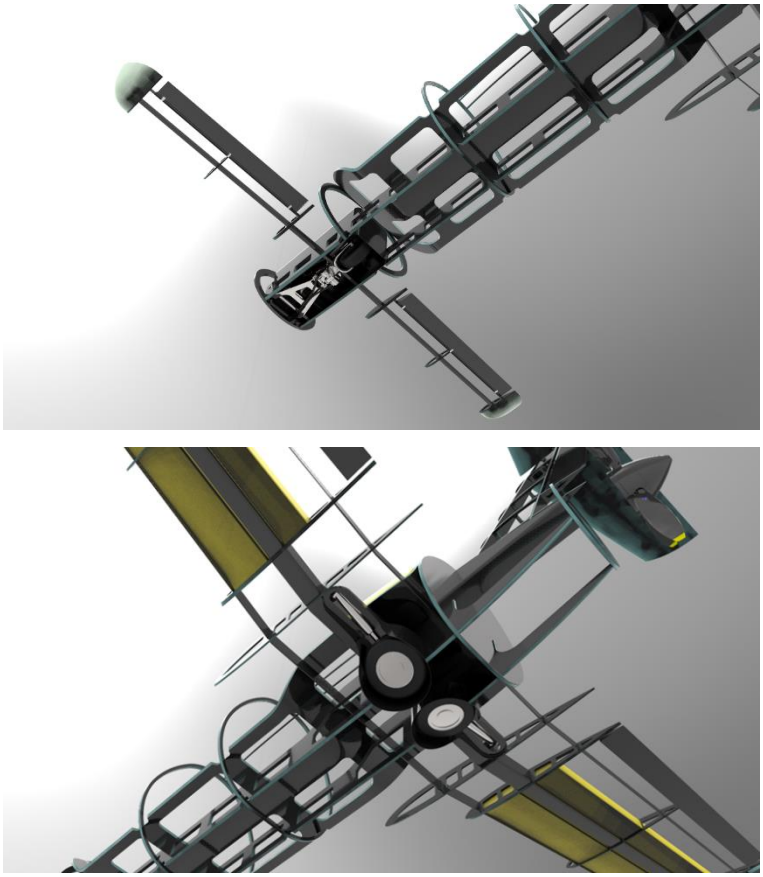

Figure 19. Landing Gear

The design of the exterior and interior of the airplane has been carried out based on the final appearance of the ODYSSEUS II, with the intention that the designer, Marc Kuster, has a feeling of what the airplane could be like and assess the need for changes or modifications.

The choice of colors has not been arbitrary. Through the broken white background, reinforced with a garnet tonality, the thesis author wanted to transmit a classic view of aviation.

In turn, the light interior, based on cream tones, aims to create a bright and spacious atmosphere.

Figure 20. ODYSSEUS II Exterior

Figure 21. ODYSSEUS II Interior

Finally, the control panel combines analogue instrumentation with the most modern of the integrated equipment, the Garmin 1000 screen.

As seen in Figure 22, in front of the pilot are the plane's governing instruments, such as the artificial horizon, the turn coordinator, the speed indicator and the vertical speed indicator.

In front of the co-pilot, there are instrumentation related to the condition of the aircraft with indicators such as fuel level, engine temperatures or manifold pressure.

Figure 22. ODYSSEUS II panel

4. AERODYNAMIC STUDIES

This section is aimed at evaluating the aerodynamic design of ODYSSEYS II aircraft. The goal of this study is to determine initially if this aircraft design is viable from an aerodynamics' point of view, followed by the studies of parameters such as lift, drag and efficiency, as well as focus on stability.

The second objective of this study is to obtain the distribution of forces that such aircraft will experience under multiple flight conditions, for the purpose of structural calculations. See section 5.1 of this document.

During the evaluation, the behaviour of the aircraft is assessed using two different methodologies.

In the first instance, the potential theory is being applied to get an initial approximation of the aircraft's behaviour using the open source software "XFLR5".

The potential theory provides relatively good results in terms of lift and moment predictions. However, being a theory of potential flow, friction drag is not taken into consideration and therefore produces somewhat erroneous results regarding drag coefficients.

To carry out a more exhaustive evaluation of this project, "CFD" technology is applied to calculate the loads with greater precision. The boundary layer viscosity produces a drag coefficient that is taken into consideration with CFD.

As a result, one obtains a higher degree of accuracy and certainty that these values are closer to reality.

The potential theory is very fast whereas the CFD methodology is more time consuming.

4.1 STUDIES METHODOLOGY

Although the overall methodology of the project has been based on loop from the aerodynamic and structural design (as presented in section 19), the specific methodology used during the design or aerodynamic study has been more pyramidal. The author of the project, departed from the requirements demanded by Mr. Kuster and the various conversations that were held, to determine the aerodynamic design in question. In turn, through the original planes of the aircraft it was possible to extract what main characteristics the Canard had to fulfil.

Although the overall methodology of the project is based on the loop principle for the aerodynamic and structural side of the design (as presented in section 2), the specific methodology used during the design and aerodynamic study is more pyramidal.

The author of this thesis started out from discussions and original plans submitted by Mr. Kuster. Using these plans, it was possible to determine the aerodynamic characteristics of this design.

Once, the exterior geometry of the front wing was determined, the modeling of the entire aircraft was carried out in 3D (See section 3), including the necessary software to perform all relevant calculations.

Multiple iterations have been carried out, first by means of the XFLR5 program and later with the CFD program, providing the answer to the question of whether this aircraft would fly or not.

4.2 THREE SURFACE AIRCRAFT PARTICULARITIES

Before going deeper into the analyses carried out, it should be mentioned the peculiarity of the airplane being studied. As the reader has already been able to observe, the plane that is being evaluated is a three surface type and there are certain considerations that must be taken into account when designing these kinds of aircraft. That is why, the author of the project has thought it appropriate to expose in a generic way the most relevant characteristics of a plane like this and that are a summary of what the reader can find in the bibliography [10], [11]

Like any existing object, the canard has certain advantages and disadvantages if it is compared to a conventional plane and varies according to the functionality or the ultimate goal of the design that is intended to be built. From the aerodynamics' point of view, a front wing set up has several disadvantages.

One of the first things to consider when designing this kind of aircraft is that the horizontal control surface is placed in front of the wing. This makes the lift of the front wing itself causes a positive pitching moment that destabilizes the plane. This factor means that to be able to stabilize the plane, statically and dynamically, and controllable, the CG must move forward compared to a conventional airplane with similar characteristics (see Figure 23). This overtaking of the CG often conflicts with the positioning of the engine, since this is usually located in the rear of the aircraft, thus expanding the destabilizing moment. The difficulty of the designer, therefore, is to be able to maintain a slope of the negative $C_{m\alpha}$ curve with a value of C_{m0} greater than 0.

Moreover, the position of the canard in front of the main wing makes the airflow that reaches the wing disturbed. This fact causes that the generated lift in those sections bathed in less clean air is produced less efficiently, thus reducing the efficiency of the whole machine and, therefore, increasing fuel consumption.

In turn, such positioning can also cause problems of non-recoverable or super-lost losses. The super lost is an aerodynamic event that occurs when being on the edge of the loss the flow detached from an aerodynamic element (canard) causes the flow of another element (wing) to be coupled, avoiding the possibility that the pilot can regain control of the aircraft.

Despite the aforementioned disadvantages, the three surface airplane also presents some advantage from the aerodynamics' point of view. Being the canard a supporting surface, this is generating a lift force that helps the wing when lifting the load. It has been calculated that the distribution of forces in a configuration like the one studied can be around $80/85\%$ for the front wing and $20/25\%$ for the canard. This fact helps to lighten the structure of the wing and helps the correct positioning of the CG.

Generally, due to the distribution of combined forces, the distribution of forces around the wing ends up having a resemblance to an elliptical distribution, which is the most efficient of the distributions.

Beyond the aerodynamic design, a canard has advantages such as a compact design or greater visibility due to the tractor engine configuration. Thus, the decision to choose what type of configuration is more appropriate resides in the designer.

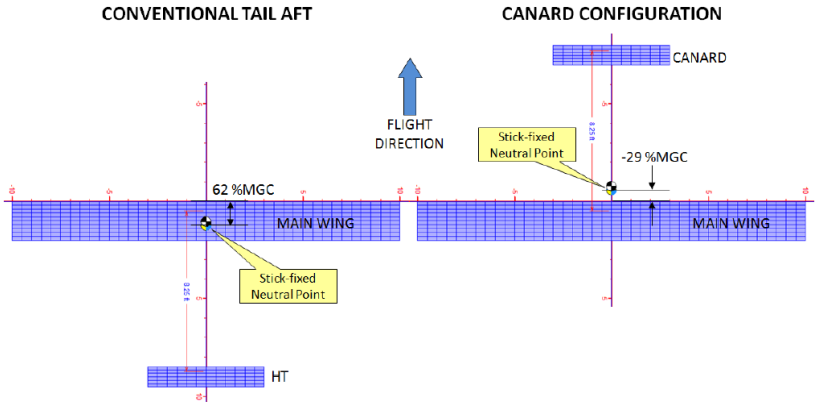

Figure 23. CG positioning comparison between a conventional aircraft and a canard. Extracted from [1].

4.3 AIRFOIL SELECTION

The envisaged wing profile chosen for the main wing and strakes is a NACA 63 series and a NACA 0010 series for the vertical fin/rudder assembly.

Burt Rutan used Eppler laminar wing profiles in his early designs of canards. These profiles provided good lift and stability under normal flying conditions. Shortcomings were subsequently discovered in rainy conditions, with to water molecules disturbing the laminar air flow and causing difficulties in pitch control at lower speeds.

For this project, the designer has chosen a John Roncz profile for the canard wing, which has proven highly successful in these designs.

Below is a summary table with the profiles used and their main characteristics.

Airfoil Characteristics				
Parameter	Symbol	NACA 63_1-412	NACA 2414	NACA 0010
Maximum Lift Coefficient	C_{lmax}	1.62	1.89	1.09
Cruise Lift Coefficient	C_{lc}	0.80	0.70	0.44
Parasite Drag Coefficient	C_{do}	0.0053	0.0056	0.0045
Zero Lift Angle of Attack	α_o	-3.00	-2.20	0.00
Stall Angle of Attack	α_s	19.00	19.00	10.00
Cruise Angle of Attack	α_c	4.00	4.00	4.00
Zero Lift Moment Coefficient	C_{mo}	-0.08	-0.05	0.00
Maximum efficiency	$(C_l/C_d)_{max}$	119	132	113

Table 1. Airfoil Characteristics. All the parameters have been calculated for a Reynolds Number of 7.000.000 (which is the Re of the cruise speed).

4.4 AIRCRAFT AERODYNAMICS' PRELIMINARY EVALUATION

4.4.1 Modelling

As mentioned above, the preliminary aerodynamic study has been carried via the XFLR5 program. Following the different analyzes carried out, some results are available below.

The first step in order to be able to evaluate how the aircraft will behave, is to transfer the geometry 2D to the calculation software. Said software, apart from generating the aircraft's geometry, lets one calculate the main characteristics and allows adjustments according to requirements of the designer.

The following program captures show the 3D geometries obtained from the original plans.

On noticeable feature in the original aerodynamic design presents a wing surface generated from the interpolation between the wing tip profile and the root profile.

This design methodology is widely used in the aeronautical sector, both at the amateur and commercial levels, since it allows obtaining wings with combined characteristics of the different profiles used.

It allows one to find solutions or mitigating various problems arising when using unconventional configurations such as a canard design. The intentionality of combining a profile with a greater lift at the tip and a more moderate profile at the root, creates an aerodynamic torsion that allows displacement of the stall entry towards the root, making the aircraft controllable throughout the entire flight envelop.

Another beneficial facet during wing design is the use of winglets. These help reduce wing tip vortices, improving aerodynamic efficiency and reducing energy consumption.

The main wing has a dihedral of 1.5 degree and a wing twist (washout) of 2 degrees throughout the entire span with the dihedral serving to improve lateral stability and washout improving stall management.

Generally, the designer seeks the best efficiency at cruising speeds and attitudes. Thus, as it is later observed, the combination of a 2 degrees incidence with an angle of attack of 4 degrees allows the aircraft to fly at maximum efficiency during the cruise stage.

Finally, the wing at root level has a short span section with a substantial chord increase. They are called "Strakes". This chord increase favors a lift improvement which counteracts to a degree the adverse effects of air flow disturbance produced by the canard.

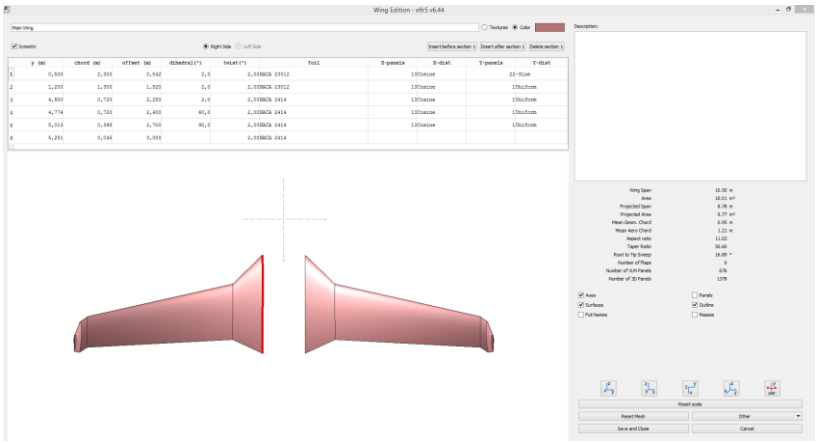

Figure 24. Wing Design. Capture from XFLR5

Regarding the canard, it can be seen how the design is rectangular and presents a certain elevation at the tip. In turn, the design presents an anhedral that aims to reduce lateral stability in this area to provide greater manoeuvrability to the aircraft.

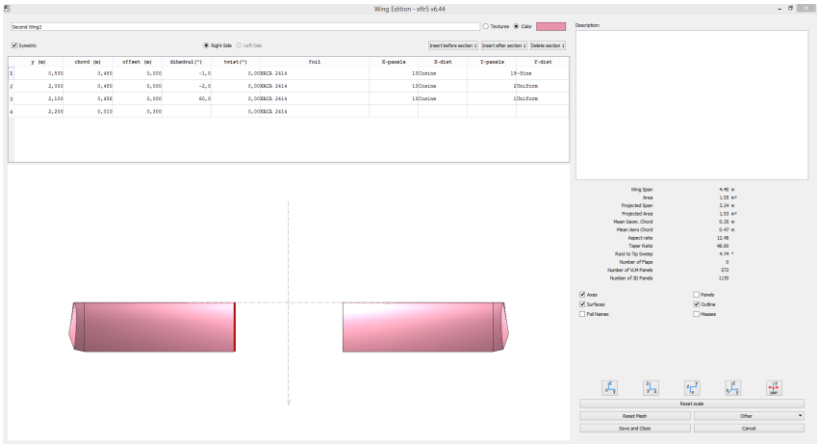

Figure 25. Canard Design. Capture from XFLR5

Of note is the fact that this concept allows for a reduction of the stall onset to between 10 and 11 Kts, which in turn translate into a reduced approach and landing speed when compared to a pure canard.

In order to guarantee lateral control of the aircraft, it is necessary to have a vertical surface that generates the required forces. Generally, in pure canard designs, the vertical fins are mounted at each tip of the main wing also providing, to a degree, a form of speed brakes, (see Burt Rutan designs, Varyeze and Longeze).

In the case of this three surface ODYSSEUS II design, the T tail concept allows for a faster yaw response.

Noteworthy also is the fact that only one vertical control surface is required, as opposed to two in the case of a pure canard. Figure 26 shows the design of the tail surfaces.

As with all designs, compromise is the order of the day and in this case there are no exceptions. What is gained in one area, is lost in another and vise e versa.

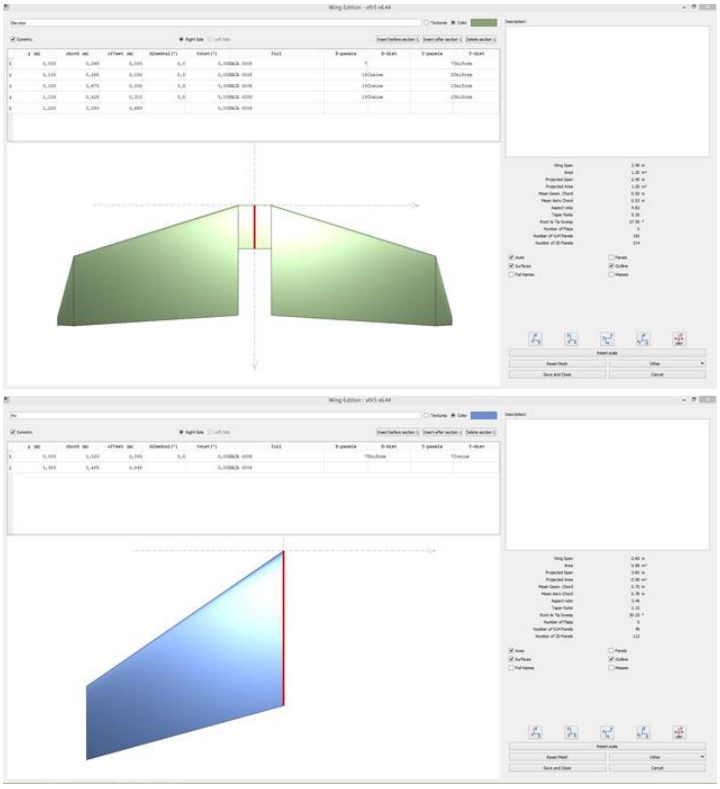

Figure 26. Tail Surfaces Design. Top: Horizontal Tail. Bottom: Vertical Tail. Captured from XFLR5.

Finally, the modelling of the fuselage surface has been carried out. For purposes of calculation, the XFLR5 does not take into account that body, so the results are always better than experimentally can be verified. In Figure 27, a simulation completed in XFLR5 can be observed, the flight conditions of which are $120\ kts$, an attack angle of $0\ deg$. And a flight level at sea level. In green, the distribution of the lift on the three supporting surfaces is observed and in purple the drag induced

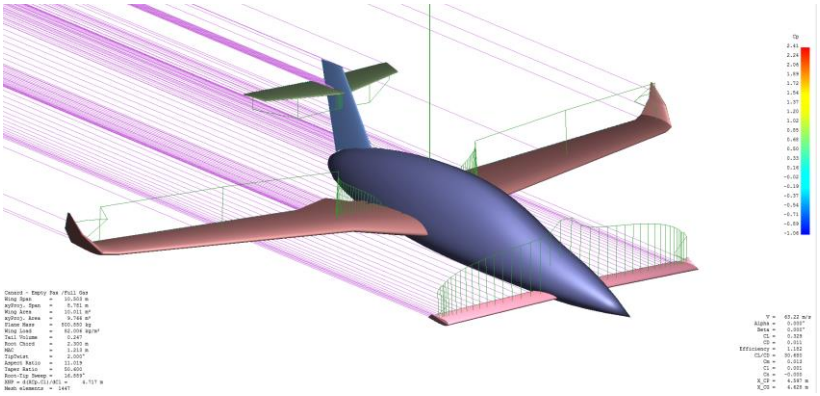

Figure 27. Full Aircraft Designed in XFLR5.

4.4.2 XFLR5 Analysis

For the purpose of analyzing the behavior of the aircraft in realistic flight situations, a series of analyzes have been carried out in combination with the structural design.

The flight conditions which have been evaluated with the results shown below, have been those the author of the project considered most essential.

VLM2 (Vortex Lattice Method 2 is the program of choice and recommended in the XFLR5 manual [4]. It is the most contrasting and most reliable. With this program, four iterations have been carried.

With a maximum all up weight of 1170 kg, four extreme configurations have been analyzed for different angles of attack, to verify the aircraft stability at any of these parameters. These are:

- Aircraft loaded with pilot plus 3 passengers and maximum fuel.
- Aircraft loaded with only pilot and maximum fuel.
- Aircraft loaded with pilot plus 3 passengers and no fuel.
- Aircraft loaded with only the pilot and no fuel.

The intentions of these analyzes is to assess any potential weak points of the canard, in respect of longitudinal/pitch stability.

Each of the conditions presents a center of gravity different from the others, allowing to obtain a broad spectrum of the plane's stability margin.

Thanks to CAD structural modeling, these four configurations have been possible and have allowed mass and inertial distributions to be introduced into the XFLR5 program.

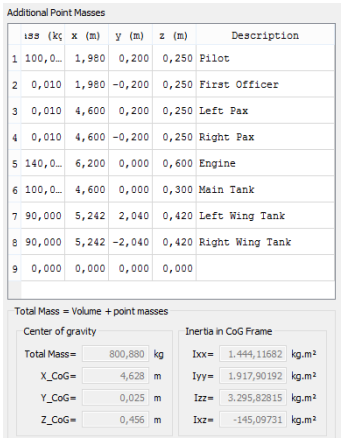

Additional Point Masses

	ass (kg	x (m)	y (m)	z (m)	Description
1	100,0…	1,980	0,200	0,250	Pilot
2	0,010	1,980	-0,200	0,250	First Officer
3	0,010	4,600	0,200	0,250	Left Pax
4	0,010	4,600	-0,200	0,250	Right Pax
5	140,0…	6,200	0,000	0,600	Engine
6	100,0…	4,600	0,000	0,300	Main Tank
7	90,000	5,242	2,040	0,420	Left Wing Tank
8	90,000	5,242	-2,040	0,420	Right Wing Tank
9	0,000	0,000	0,000	0,000	

Total Mass = Volume + point masses

Center of gravity

Total Mass=	800,880	kg
X_CoG=	4,628	m
Y_CoG=	0,025	m
Z_CoG=	0,456	m

Inertia in CoG Frame

Ixx=	1.444,11682	kg.m²
Iyy=	1.917,90192	kg.m²
Izz=	3.295,82815	kg.m²
Ixz=	-145,09731	kg.m²

Figure 28. Example of mass distribution.

Below are the aerodynamic curves resulting from the different analysis carried out. As shown in the $C_L - \alpha$ (figure 29), the different weight configurations studied do not significantly affect the overall lift of the aircraft. It can be observed in said graph, that below an angle of attack of $8\ deg.$, the aircraft is still in a linear regime, with a maximum support of 1.2. In said graph it is not shown at which angle the airplane stalls. This event is evaluated in the corresponding section.

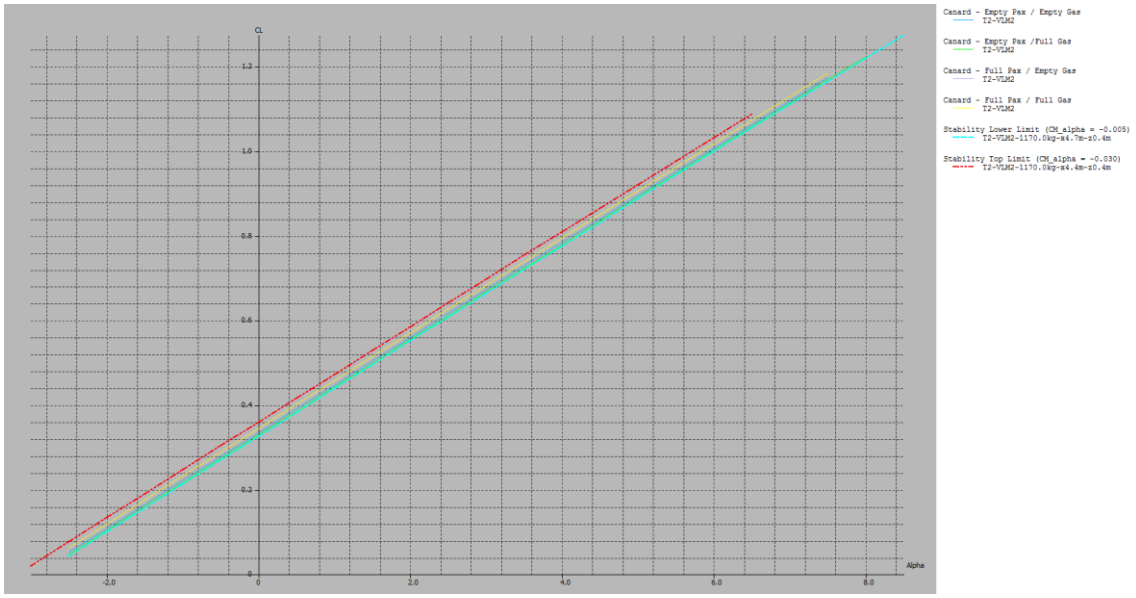

Figure 29. $C_L - \alpha$ Curve. Extracted from XFLR5

In the polar curve (figure 30), it can be seen that, as in the first curve, the values obtained for the different configurations do not differ much. In turn, it can be mentioned that said polar curve is not very relevant, since as mentioned previously the viscous drag has not been taken into account. So that the reader can have a sense of how wrong one is, it must be said that the Cessna 172 has a parasite drag (minimum drag on the polar curve) of approximately 0.02. Fixing us on the obtained graph, it can be seen how the canard that is being designed presents a parasite drag 0.01.

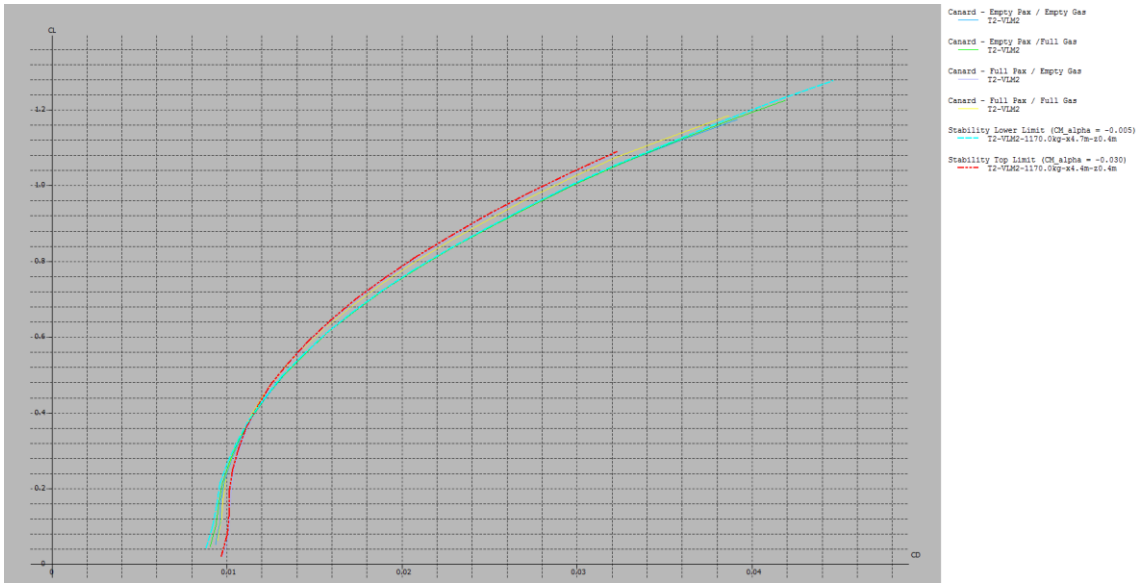

Figure 30. Polar Curve. Extracted from XFLR5.

Looking at the aerodynamic efficiency curve, it can be seen how it increases as the aircraft weight goes up.

This is due to the increase in lift required to compensate for the increase in total weight, when the aircraft flies in a balanced manner. Such a rise is much higher than the increase in aerodynamic drag.

From this graph, one can conclude that the aircraft must fly trimmed with an angle of $2.5\ deg.$ for maximum flight efficiency.

This information helps when designing the wing, since the incidence (or rigger's angle) can be varied in order to control the angle at which the aircraft flies in a level attitude.

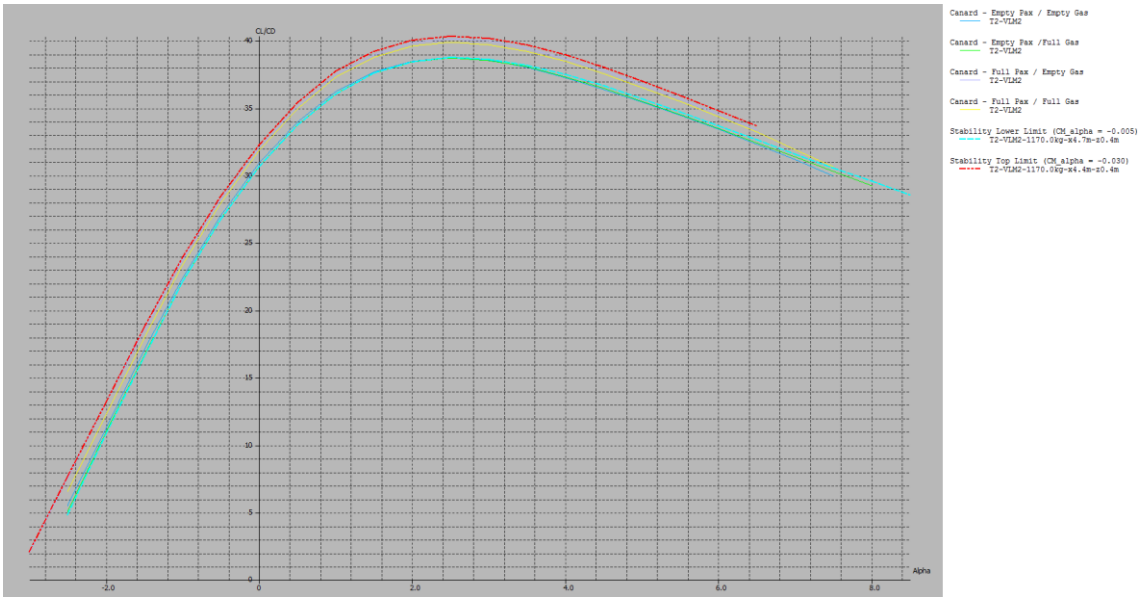

Figure 31. Aerodynamic Efficiency Curve. Extracted from XFLR5.

The following graph is one of the most important at the level of study that can be obtained from the XFLR5. This graph details the pitching moment of the airplane and, therefore, it can be studied if it is statically stable or not. According to Torenbeek [13], a good criterion of stability when carrying out preliminary studies and designs of aircraft is that the airplane must have positive C_{m0} and a slope between $-0.005\ deg.^{-1}$ and $-0.030\ deg.^{-1}$.

These limits are shown in the graph as two discontinuous red and cyan lines. As can be seen, the canard designed by Mr. Kuster meets both criteria under any of the cases provided as long as the aircraft is trimmed correctly. In table 2, it is possible to observe the angle of trim of the elevator and the canard that are needed so that the airplane is statically stable under the extreme conditions proposed.

As these angles are not excessive and are easily obtainable by means of a good trim system, it can be concluded that the canard is statically stable.

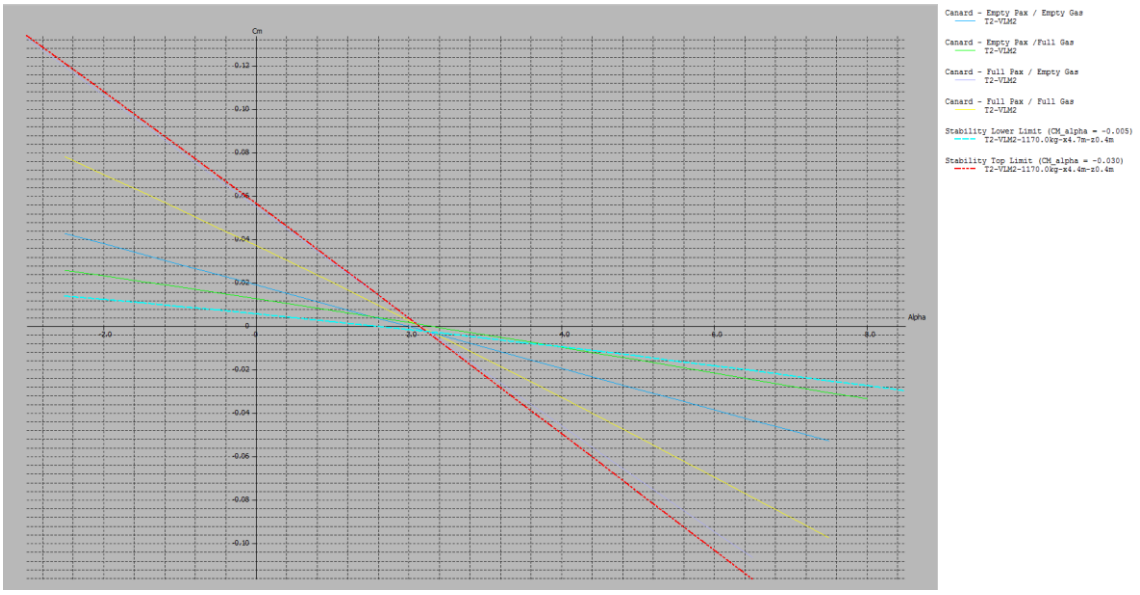

Figure 32. $C_m - \alpha$ Curve. Extracted from XFLR5.

Moment Coefficient and Trimming Angle				
Configuration	C_{m0}	$\frac{dC_m}{d\alpha}$	Elevator Trimming Angle	Canard Trimming Angle
Full Passenger / Full Fuel	0.037	-0.017	-2.0	2.0
Only Pilot / Full Fuel	0.013	-0.006	-1.1	1.1
Full Passenger / Empty Fuel	0.055	-0.026	-2.8	2.8
Only Pilot / Empty Fuel	0.019	-0.009	-1.4	1.4

Table 2. Moment Coefficient and Trimming Angles.

Another very important graph is the one shown in figure 33.

This shows the lift coefficient needed for the aircraft to fly at a given level and a specific speed. This graph allows one to assess whether the aerodynamic design meets or not the requirements for the speeds proposed in requirements section of this document.

As can be seen, the minimum flight speed, that is, the stall speed of the aircraft, is below $45\ Kts$. This is a clear indication that the design meets the initial requirements, as it was required that the entry speed in lost with clean configuration, ie, without flaps, and for any load condition should be below $52\ kts$.

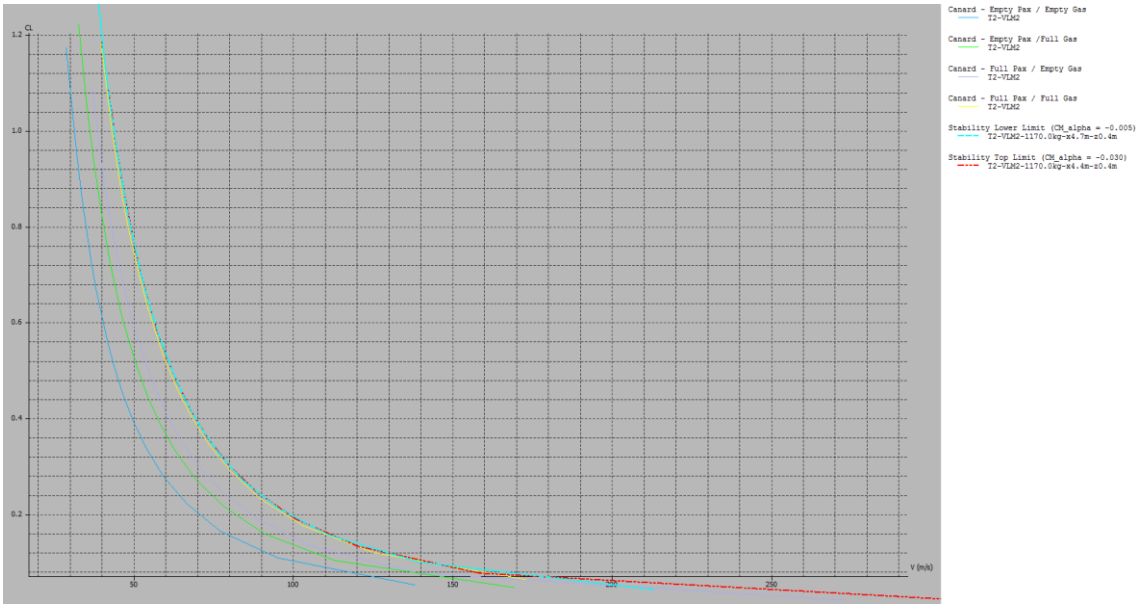

Figure 33. C_L versus speed curve. Extracted from XFLR5.

4.5 COMPUTATIONAL FLUID DYNAMICS

In this section the detailed aerodynamic study of the canard is presented. To do this, the CFD methodology has been used through the CFX application of the commercial software Ansys 17.

The analyses carried out have been based on numerical simulations of the aircraft for ranging stall speed ($50\ Kts$) to never exceed speed ($250\ Kts$). The angle of attack of the aircraft has been varied from -$10\ deg.$ to $10\ deg.$ in order to obtain enough points to represent the characteristic curves of the aircraft.

The CFX module has been configured to use discrete pressure-based solver (widely used for incompressible flow problems). For the discretization of the flow, a second-order upwind scheme has been used, while for the turbulence simulation "Turbulent Kinetic Energy" first-order scheme has been applied.

As convergence criterion RMS, $1e^{-4}$ has been designated. The purpose of the configuration of the software is to obtain decent results, but in a fast way due to because these are first iterations of the design.

For boundary conditions a cubic space has been recreated which each side measures 4 times the span of the plane. This cube is in undisturbed conditions with a velocity of $0\ Kts$, a pressure of $1\ atm$ and a density of $1{,}225\ kg/m^3$, pretending to simulate the conditions at sea level. At the inlet wall, the applied velocity corresponds to which the plane is flying.

The modelling of the surface has been carried using CATIA V5. The external surface of the airplane has been simplified, avoiding elements such as windows, propellers or antennas as shown in Figure 34. Subsequently, it has been meshed by the Mesh module of Ansys 17, with refined mesh parameters.

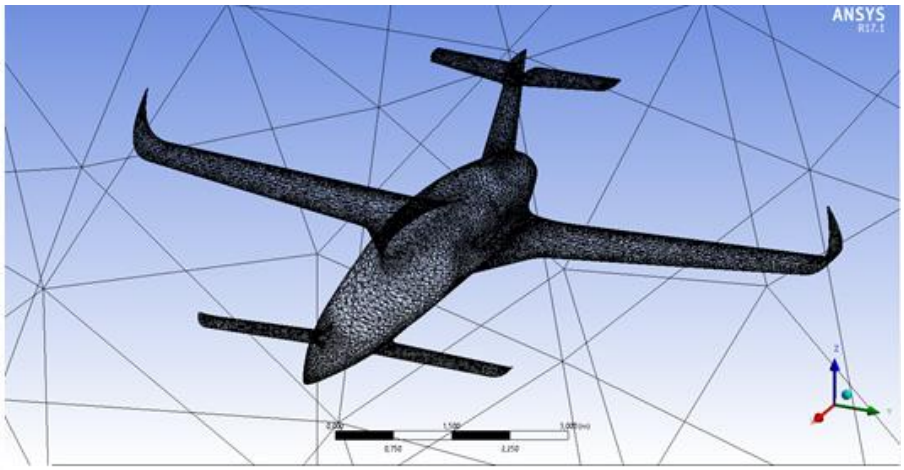

Figure 34. Left: CATIA V5 Model. Right: Ansys 17 Mesh

The Ansys CFX module allows obtaining the aerodynamic forces that affect the aircraft in the XYZ directions.

However, to be able to extract the characteristic curves, a post-process has been carried out in Excel, with which the drag forces and drag coefficients as well as aerodynamic coefficients have been calculated.

The following table shows the values used to carry out these calculations, including the equations used.

$$L = Fz \cdot \cos(\alpha) - Fx \cdot \sin(\alpha) \quad (1)$$

$$D = Fz \cdot \sin(\alpha) + Fx \cdot \cos(\alpha) \quad (2)$$

Canard CFD Parameter		
Parameter	Symbol	Value
MTOW	$MTOW$	1170 kg
Wing Surface	S_w	10.01 m^2
Wingspan	B_w	10.50 m
Mean Aerodynamic Chord	MAC_w	1.21 m

Table 3. Canard CFD Parameter. Extracted from XFLR5

The obtained results are showed next. In the $C_L - \alpha$ curve it can be seen how the obtained lift values are similar to those obtained in the XFLR5.

Although it is true that the values are slightly lower than those of XFLR5, these results can be considered favorable, therefore providing a satisfactory first estimate of the aircraft's behavior.

Using the CFD program, some divergences in values show up, due to the fuselage.

For obvious reasons the airflow disruptions created, affect the angle of maximum lift coefficient. With the potential theory, the coefficient lift value is 1.2 to $8\ deg$.. For the calculation in the CFD program, the value obtained is $10\ deg$.

Focusing on the polar, it can be observed as now, the viscous drag has been taken into account by raising the parasite drag coefficient (parameter used as a reference) from 0.01 to 0.05. This increase of the drag causes a decrease in the aerodynamic efficiency as shown in figure 37.

According to the results of the Ansys 17, the maximum efficiency of the airplane is approximately 9 and it is placed around $4\ deg$.. Although it is not a very high efficiency value, it is a value that falls within normal limits for this type of aircraft, especially considering that it is a canard whose disadvantage is the lower efficiency compared to a conventional aircraft.

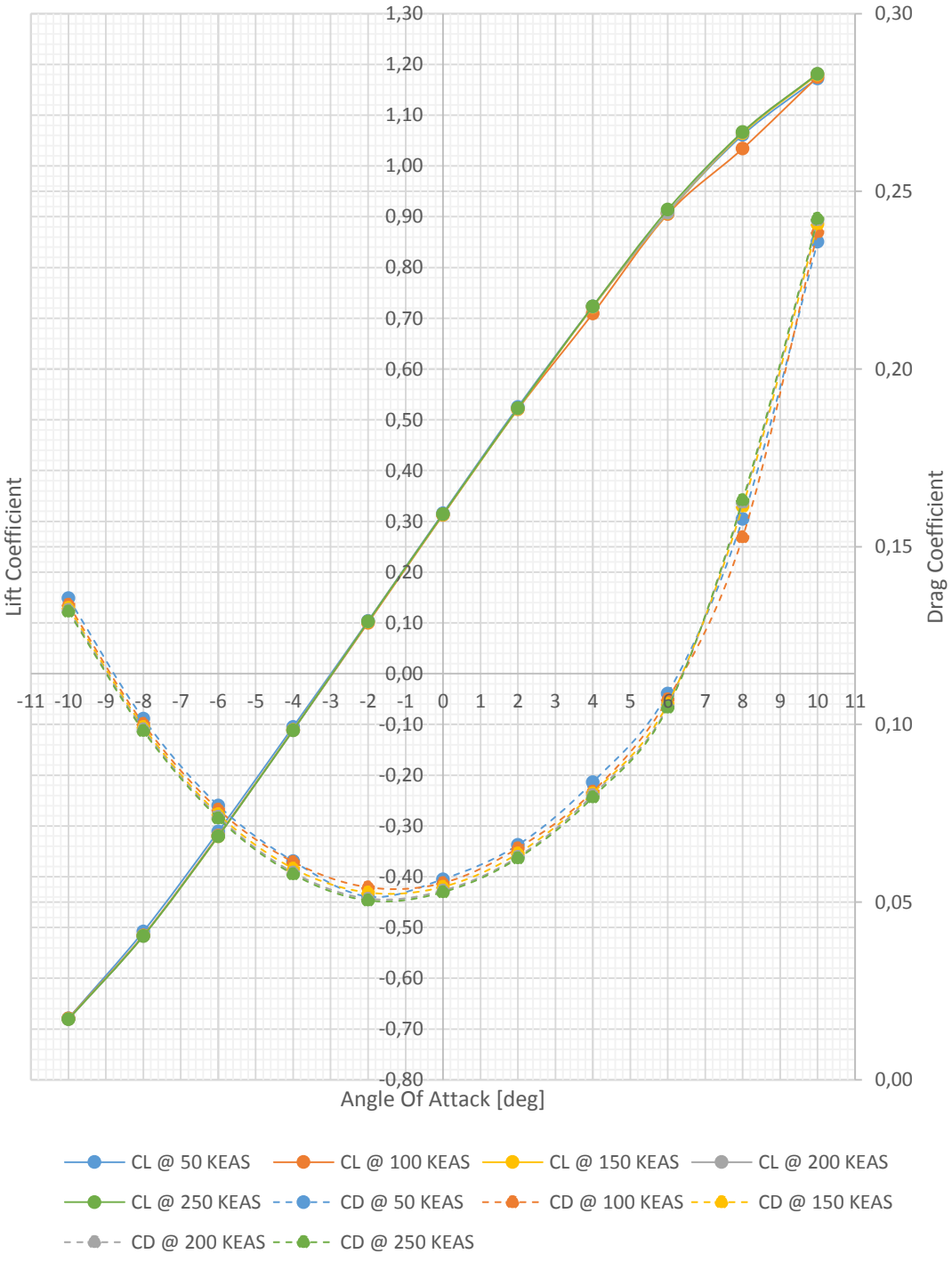

Figure 35. CFD Aerodynamic Coefficients

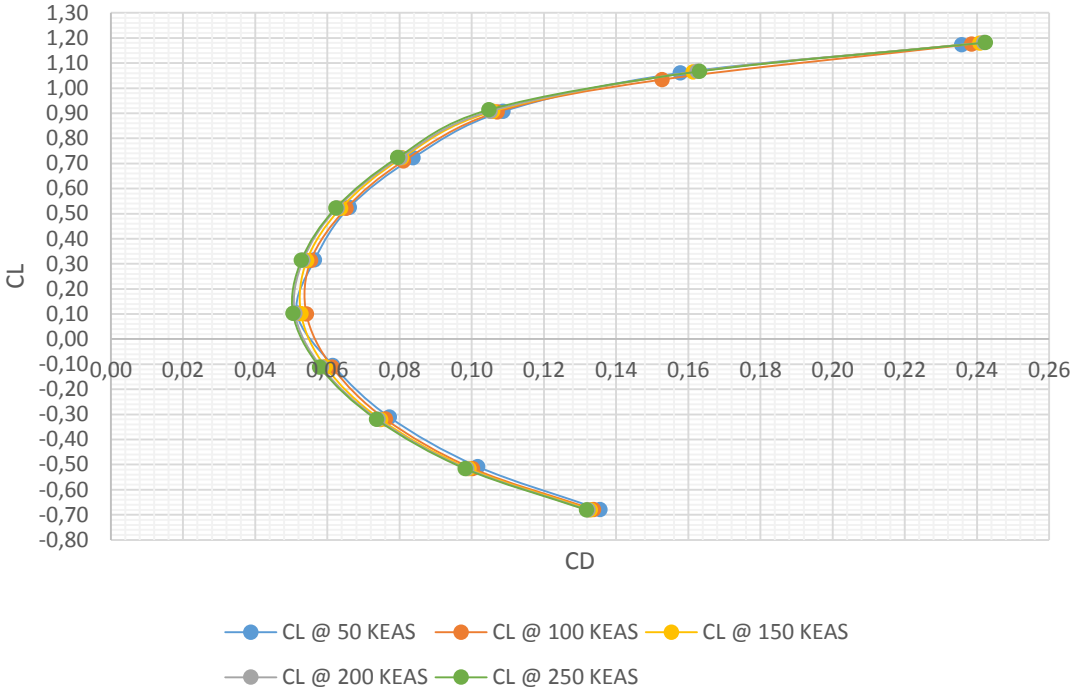

Figure 36. CFD Polar Curve.

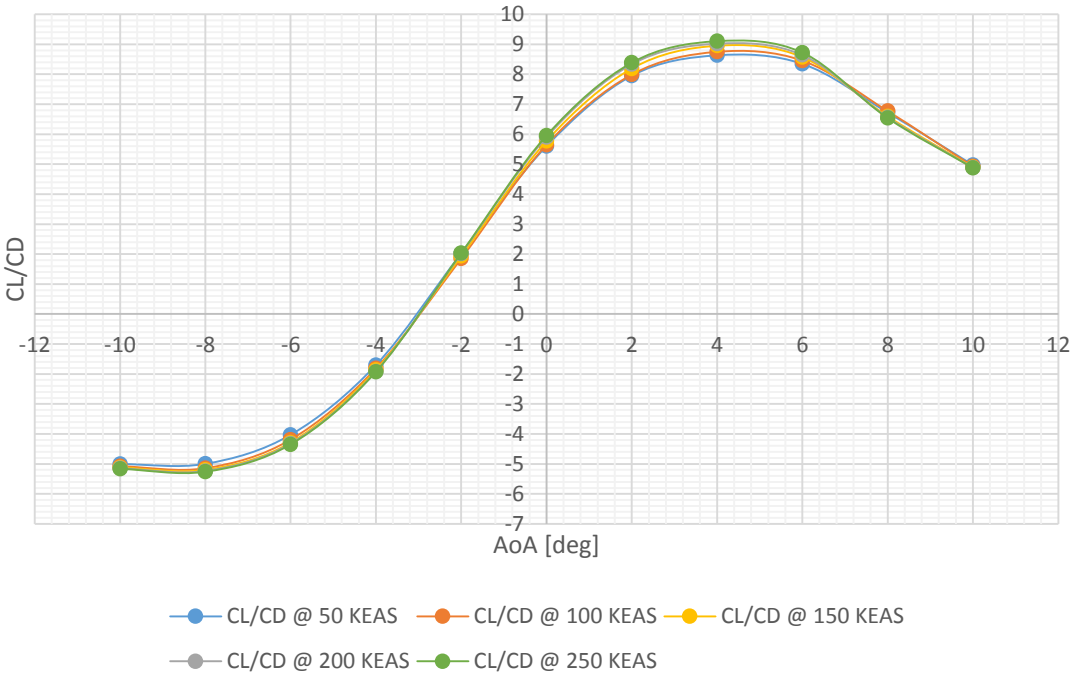

Figure 37. CFD Aerodynamic Efficiency

Another of the studies that is possible to realize thanks to the CFD analysis is the one that compares the drag with the speed and the angle of attack.

Using the graph in figure 38, it is possible to cross-link the thrust curve of the engine to assess whether the aircraft is capable of flying with the chosen engine and in the indicated flight conditions.

As the propulsive study is outside the scope of the project, a fictitious propulsion curve has been provided to illustrate what the study process would look like. However, the drag values presented are those calculated during the CFD analysis performed.

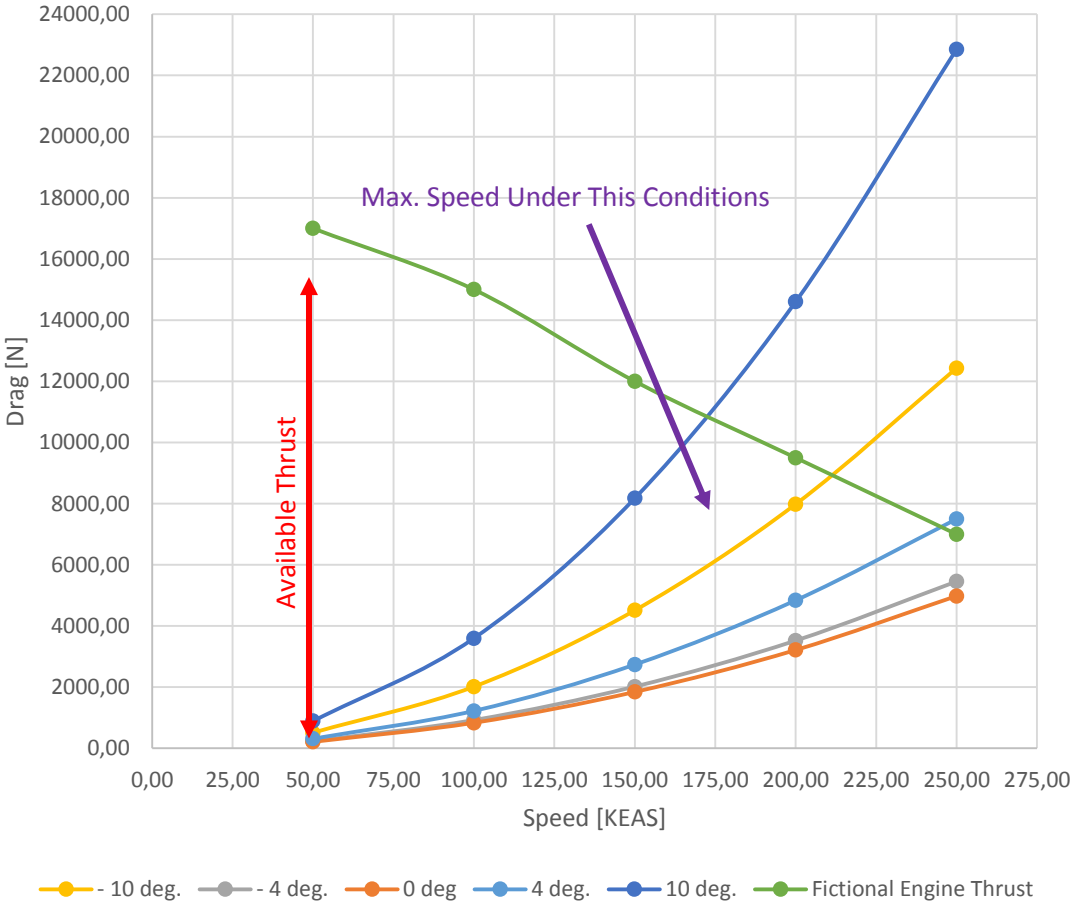

Figure 38. CFD Drag vs Speed

Finally, a qualitative study of the stall behavior of the aircraft has been carried out. This study is very important since the occurrence of the stall onset is key to ensuring that the aircraft is safe and controllable in such an event.

In order for an aircraft to have a stall as controllable as possible, such stall has to start at the wing root and progressively move toward the wing tip. As mentioned earlier, the main wing never reaches a stall situation. The canard is the wing surface that will let go, so to speak.

Abrupt stalls are never a comfortable occurrence whether to a novice, experienced and or even seasoned pilot. There are ways of softening such stall behaviors. One of them, mentioned earlier, is the use of "Washout".

The negative aspect of washout is a certain amount of lift loss at wing tip level. This happens due to the root chord line having a higher value compared to the chord line of the wing tip. But the positive side of it is a more gradual stall moving from root to tip.

The norm for washout is between 2 and 3 degrees.I t follows that with this scenario the wing tip flies at 2 to 3 degrees less angle of attack. Hence, the loss of aerodynamic efficiency of the surface in question.

In this project, the designer has chosen a 2 degree washout, which is ample to insure total safety against a potential wing stall. Since in this particular design, the only wing surface allowed to stall is the canard, a milder stall behaviour can also be welcomed.

All the above information confirms that this aerodynamic design is valid and is a solid base for envisaging the construction of such a craft.

There are no adverse circumstances throughout this projected flight envelop that can affect the controllability in any negative manner.

On a side note, there is an interesting aspect of the canard concept, in as such that the airflow disturbance caused by the canard affects the main win at root level.

This causes the air flow at the leading edge of the main wing to be turbulent which favors the subsequent detachment of the boundary layer on said main wing.

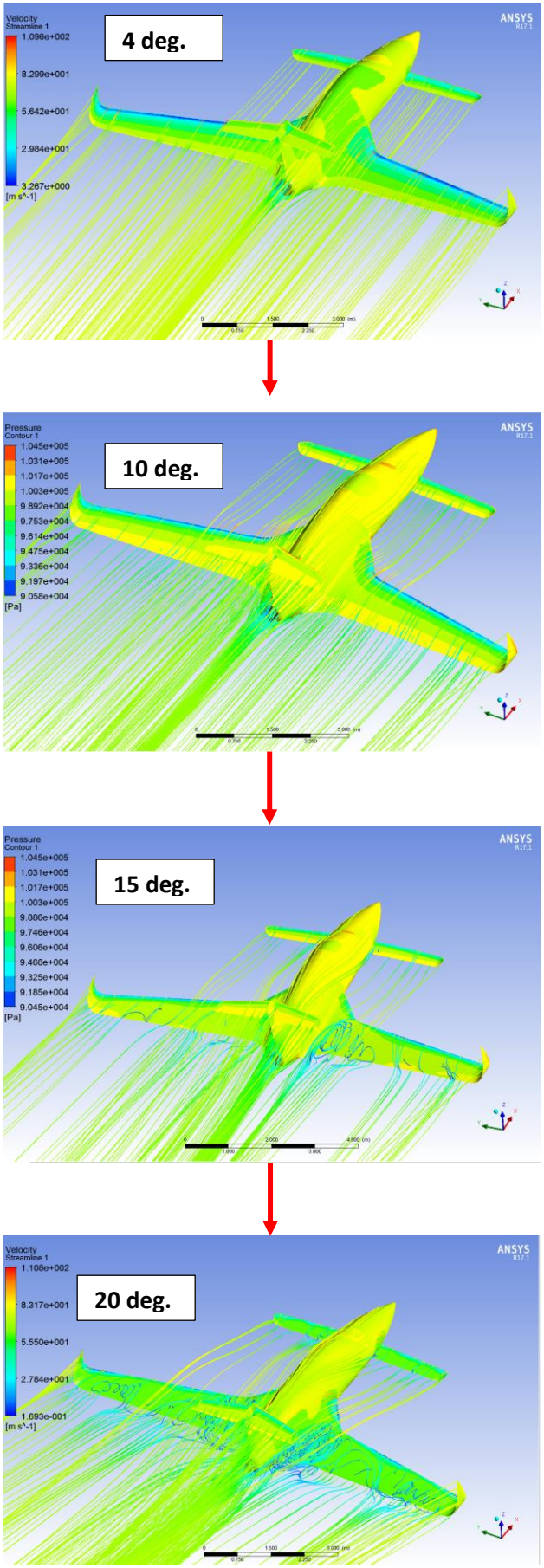

Figure 39. Stall Studies

5. STRUCTURAL STUDIES

In this section the various studies and calculations that have been carried out in order to obtain a first pre-dimensioning of the structure of the aircraft, and an assessment of the most critical parts under the most extreme conditions are exposed.

The methodology that has been used to carry out these analyzes has been based on the methodology used in the final degree thesis of the author of this study (see reference [15]), and which is explained below.

The steps to follow to pre-sizing the structure are 4:

1. Study of the loads in the most extreme situations. This step consists of calculating the aerodynamic loads to which the aircraft must face based on its flight envelope. For this, said envelope is previously calculated.
2. Analytical pre-sizing. Through different Matlab codes developed in the framework of the previous thesis, and improved for the development of this thesis, several analytical calculations are carried out to obtain the main parameters of the structure.
3. Modeling and analysis in Finite elements. This section consists of analyzing the previously developed 3D model. Depending on the degree of detail of the study, the values will be closer to the real behavior of the structure tested.
4. Redesign those elements that show unfavorable results compared to the tests carried out.

The calculations developed in this section have been linked to the aerodynamic studies of the previous sections, as mentioned in the exposition of the thesis methodology.

5.1 FLIGHT ENVELOPE

As previously mentioned, the first step to be able to size a structure is to know what the loads it must support are. For this, it is essential that the most extreme conditions to which the structure can work are calculated.

In the aeronautical sector, an essential graph during the design of an aircraft is the flight envelope. This figure relates the efforts (evaluated in G forces) in relation to the speed of the aircraft.

These relationships are determined by the different related regulations. In the case of the ODYSSEUS II, although it is an experimental aircraft, the CS23 standard has been applied for aerobatic aircraft, as it is the most demanding and, therefore, the one that guarantees greater structural safety.

Following the methodologies of references [2], [16] and [17] the flight envelope for ODYSSEUS II has been developed, using the code in Annex 10.1. The parameters used are shown in Table 4.

Flight Envelope Parameters			
Parameter	Symbol	Unit	Value
Max. Lift Coeff.	$C_{L_{\max}}$	-	1.20
Full Flap Aircraft Lift Coeff.*	$C_{L_{FF}}$	-	1.44
Take-off Aircraft. Lift Coeff.*	$C_{L_{Fto}}$	-	1.38
Aircraft Min. Lift. Coeff.	$C_{L_{min}}$	-	-0.70
Wing Surface	S_W	m2	10.01
Mean Geometric Chord	MGC	m	0.95
Maximum Take-off Weight	W_{to}	kg	1170
Minimum Flying Weight	$W_{\min}$	kg	729
Minimum Flying Weight Full Fuel	$W_{\min_{ff}}$	kg	952
Max. Positive Load Factor	n_1	-	+6
Max. Negative Load Factor	n_2	-	-3

*Table 4. Flight - Envelope parameters. * The values of Lift Coefficient Related with flaps have been estimated as an increment of 30% of the lift coefficient according to reference [2].*

The flight envelope requires that the different airplane speeds are calculated, defined below.

Maximum Speed in Level Flight

It is considered the maximum speed defined in the requirements,

$$V_H = 220\ KEAS$$

Stall Speeds

It are considered four stall speeds for the four principal flight configurations of the aircraft. This speeds must be proved in flight as the requirement 4.4.1 of the reference [17] dictate,

Flaps retracted (cruise configuration)

$$V_s = \sqrt{\frac{2W_{to} \cdot g}{\rho_o C_{Lmax} S_w}} \tag{3}$$

Flaps full extended (landing configuration)

$$V_{so} = \sqrt{\frac{2W_{to} \cdot g}{\rho_o C_{LmaxFF} S_w}} \tag{4}$$

Flaps partial extended (Take-off configuration)

$$V_{s1} = \sqrt{\frac{2W_{to} \cdot g}{\rho_o C_{LmaxFto} S_w}} \tag{5}$$

Flaps retracted (Inverted cruise configuration)

$$V_{s2} = \sqrt{\frac{2W_{to} \cdot g}{\rho_o |C_{Lmin}| S_w}} \tag{6}$$

Design Manoeuvring Speeds

The next speed to define is the design manoeuvring speed. According to requirement 5.2.4.1 [17] which is defined by the expression 7,

$$V_A = V_S\sqrt{n_1} \tag{7}$$

Flap Maximum Operating Speed

The flap maximum operating speed must be equal to or greater than the highest speed defined by the expressions 23 and 24 according to 5.2.4.2 [17],

$$V_{\max F} = 1.4V_S \tag{8}$$

$$V_{\max F} = 2V_{SO} \tag{9}$$

Flap Maximum Extended Speed

It is chosen the flap maximum extended speed the same as the flap maximum operating speed.

Design Cruise Speed

According to requirement 5.2.4.3 [17], the cruising speed must be chosen within the limits established by the equation 10 and 11,

$$V_{Cmin} = 4.77\sqrt{\frac{W_{to}\cdot g}{S}} \tag{10}$$

$$V_{Cmax} = 0.9V_H \tag{11}$$

Design Dive Speed

According to requirement 5.2.4.4 [31] the minimum dive speed must be,

$$V_D = 1.4V_{cmin} \tag{12}$$

Never Exceed Speed

This speed should be equal to or greater than 1.1 cruise speed, and must be equal to or less than 0.9 dive speed.

Once the different speeds of the aircraft are calculated, the gust loads are computed. For this, the calculation method proposed in appendices of [15] is used. The appendix also states that for cruise speed a gust of 15 m/s should be considered, whereas a 7.5 m/s gust must be considered for dive and flaps extended flights.

Thus, using the expression 13, the loads produced by the gust are evaluated for different weights of the aircraft (maximum weight, minimum flying weight and minimum flying weight with full fuel). Then, the maximum gust load factors are drawn in the flight envelope.

$$n_{3/4} = 1 \pm \frac{\frac{1}{2}\rho_o k_g V a U_{de}}{\frac{W}{S}} \tag{13}$$

Where $a = \left(\frac{dC_L}{d\alpha}\right) = 4.97\frac{rad}{s}$, $k_g = 0.88 \cdot \frac{\mu_g}{5.3+\mu_g}$ and $\mu_g = \frac{2W}{\rho_o MGCaS_w}$

In Figure 40, the flight envelope of ODYSSEUS II calculated by the code of Annex 10.1 is observed.

The values obtained show how the most extreme situations consist of the upper and lower limits of the maneuvering curve. This is because by requiring that the load factor values be + 6 / -3.

On the other hand, it can be seen how the most extreme value of all is that in which the plane flies at maximum speed with the maximum G positive. This point is the one that will be used to analyze the structure of the aircraft

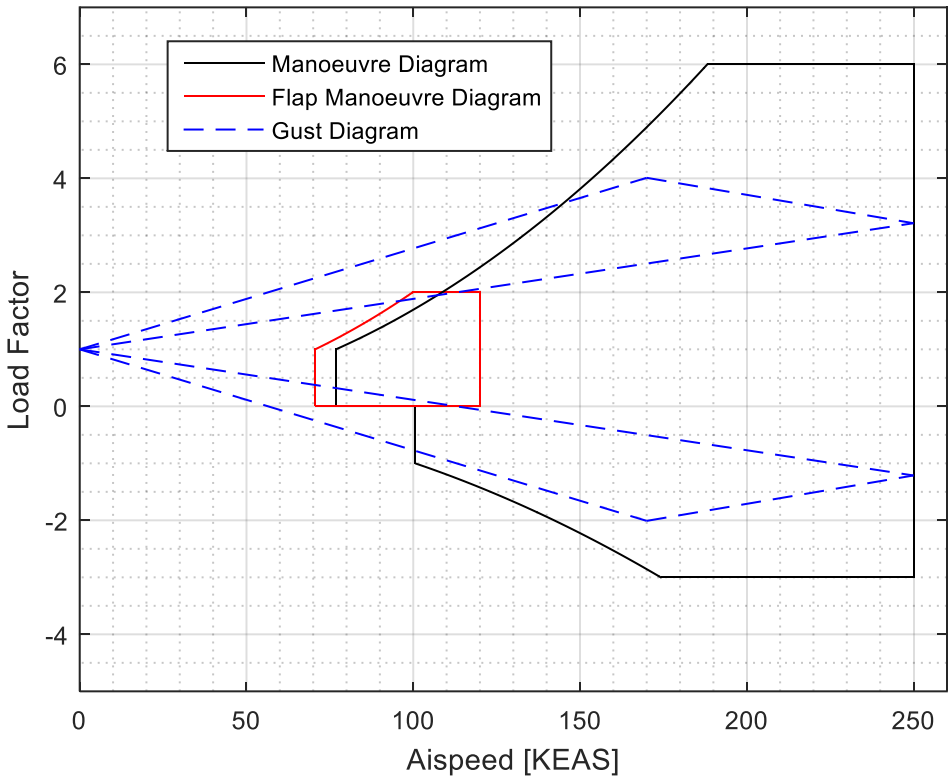

Figure 40. ODYSSEUS II Flight Envelope

5.2 STRUCTURE PRE-SIZING

The process that is exposed below is extracted from the reference [15], which corresponds to the thesis of the degree of the author of the project.

Said that, the analysis carried out below are considering a level flight with symmetric loads under different Gs conditions.

To carry out a first estimation of the structural design in order to calculate the different thicknesses necessary for the structure to resist, the assumptions of the reference [2] are used. In it, the wing is idealized as a D composed of a skin, two caps and a shear web. The first is responsible for supporting the torque moment, the caps of the beam are in charge of the bending moment and shear web holds the shear efforts, as shown in figures 41 and 42.

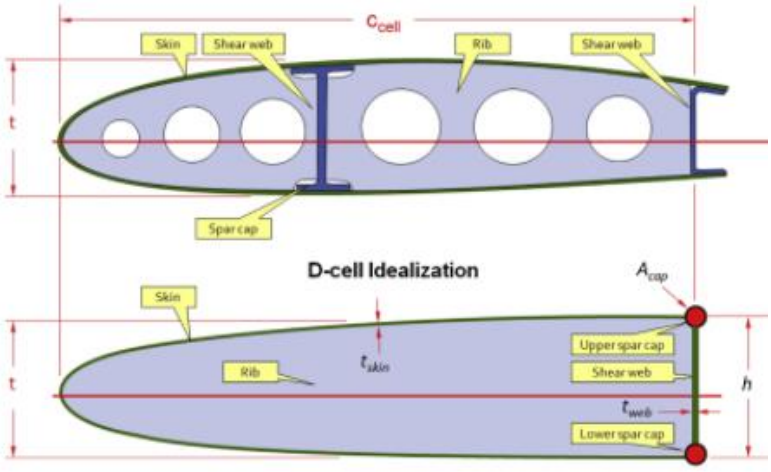

Figure 41. Wing Section idealization. Extracted from [2]

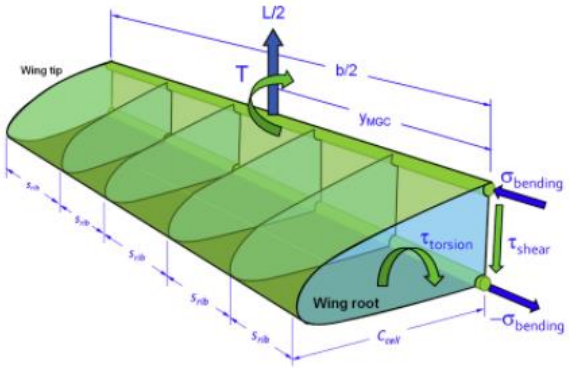

Figure 42. Loads in the idealized wing. Extracted from [2]

The thickness of the skin is calculated by following the procedure described below. For this, it is considered that entire torque is fully supported by the skin, and is calculated by the expression 29.

$$T = \frac{1}{2}\rho V_D^2 \frac{Sw}{2} \cdot MGC \cdot |Cm| \tag{14}$$

From the expression of the shear stress in the root can be extracted the thickness of the skin as,

$$t_{skin} = \frac{|T|}{2A_{cell}\tau_{max}} \tag{15}$$

The area of the idealized cell is defined as,

$$A_{cell} = \frac{4C_{cell}h/3}{3} \tag{16}$$

Where C_{cell} is the root chord minus the flap and h is the airfoil thickness.

Finally, the maximum shear stress is defined as the maximum tensile strength of the material divided by the shear strength of 1.5 indicated by the CS-LSA snd CS-23 standards.

$$\tau_{max} = \frac{\tau_{glassfiber}}{FS} \tag{17}$$

The calculation of the shear web thickness is performed considering that the shear stress is reacted entirely by this and that the maximum requirement is in the root. Thus, the shear effort is defined as,

$$V = \frac{1}{2} n_{max} W \tag{18}$$

The shear web thickness can be obtained from the expression of the shear stress.

$$t_{web} = \frac{3}{4} \frac{n_{max} W}{h \tau_{max}} \tag{19}$$

As before, the maximum shear stress is defined as,

$$\tau_{max} = \frac{\tau_{carbon}}{FS} \tag{20}$$

The procedure of obtaining these expressions is described in reference [2].

For the bending moment, the author has considered to carry out a decomposition of the effort in a more exhaustive way. That is why, following the model proposed in the reference [19], has the lift force has been idealized as an elliptical load acting on the front beam. To this load has been added the own weight of the structure and the amount of fuel that is carried in the wings.

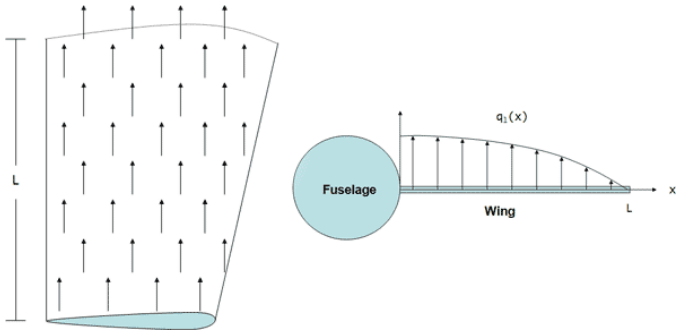

Figure 43. Idealized lift distribution. Extracted from[19].

The equations describing the applied loads are as follows.

$$ql(x) = \frac{2Wn_{max}\sqrt{b_{ref}^2 - x^2}}{\pi b_{ref}^2} \quad (21)$$

$$q_{cap}(x) = -\frac{\rho_{cap} A_{cap} b_{ref}}{nel} \quad (22)$$

$$q_{skin}(x) = -\frac{\rho_{skin} \frac{S_w}{2} t_{skin}}{nel} \quad (23)$$

$$q_{web}(x) = -\frac{\rho_{web} b_{ref}}{nel} \quad (24)$$

$$q_f(x) = -\frac{W_f}{2b_f} \quad (25)$$

Where $b_{ref} = \frac{b_w - w_f}{2}$

From these equations and applying the matrix theory of structures exposed in references [19] and [20] the code of Annex 10.2 is developed to analyse various situations and to obtain the necessary thicknesses to hold the loads depending on the material used.

5.2.1 Main Wing Sizing

To pre-size the structural elements of the main wing, the data chosen in the following table have been used.

It has been considered that the main wing generates a lift of 75% of the overall lift of the aircraft. In turn, the structure has been analysed without counting the weight of the fuel in the wings, as this is an element that helps reduce the load to which the structure is subject.

Main Wing Pre-sizing Parameters			
Parameter	Symbol	Unit	Value
Max. Take-off Weight	$MTOW$	kg	877.5
Mean Geometric Chord	MGC	m	0.95
Wing Surface	S_W	m^2	10.50
Airfoil Thickness	t_{airf}	%	12
Wingspan	B_w	m	10.01
Reference Moment Coefficient	$C_{m_{ref}}$	-	-0.186
Security Factor	FS	-	3
Wide Spar Cap	w_{cap}	m	0.12
Estimated Cap Thickness	t_{cap}	m	0.02
Load Factor	n	-	6

Table 5. Main Wing Pre-sizing Parameters.

The characteristics of the material used have been obtained from the reference [2]. The homogenized properties of an epoxy-based composite material and reinforcements in carbon fiber, and another with epoxy base and fiberglass reinforcements have been used.

The properties of both materials are shown in the following table.

Materials' Mechanical Properties				
Parameter	Symbol	Units	Carbon Fibre + Epoxy	Glass Fibre + Epoxy
Density	ρ	kg/m^3	1590	1770
Young Modulus	E	GPa	67.6	24.8
Ultimate Yield Tensile	σ_{ult}	MPa	835	320
Ultimate Shear Tensile	τ_{ult}	MPa	97	99

Table 6. Materials' Mechanical Properties

The results obtained after carrying out the necessary calculations are shown in the following table.

In the first place, the minimum skin value necessary to support the load values for the most extreme flight conditions of the flight envelope calculated in section 5.1 has been obtained.

In turn, the table also shows the maximum displacement of the wing tip.

Main Wing Sizing Results			
Parameter	Skin Thickness [mm]	Shear Web Thickness [mm]	Tip Vertical Displacement [mm]
Speed: 250 Kts n: +6 G	2.96	10.30	578
Speed: 250 Kts n: -3 G	2.96	5.15	-289
Speed: 70 Kts n: +1.5 G	0.22	2.57	129
Speed: 100 Kts n: -1 G	0.44	1.71	87

Table 7. Main Wing Sizing Results.

As can be seen, the most extreme case and that requires higher thicknesses is the one made at $250\ kts$ and with a load factor of $+6$. These conditions are those used to size the structure, with the values obtained, and are the boundary conditions that will be used during the FEM analyzes.

The following figure shows the different distribution of loads and the response of the structure obtained after the analysis of $250\ kts$ and $+6\ G$.

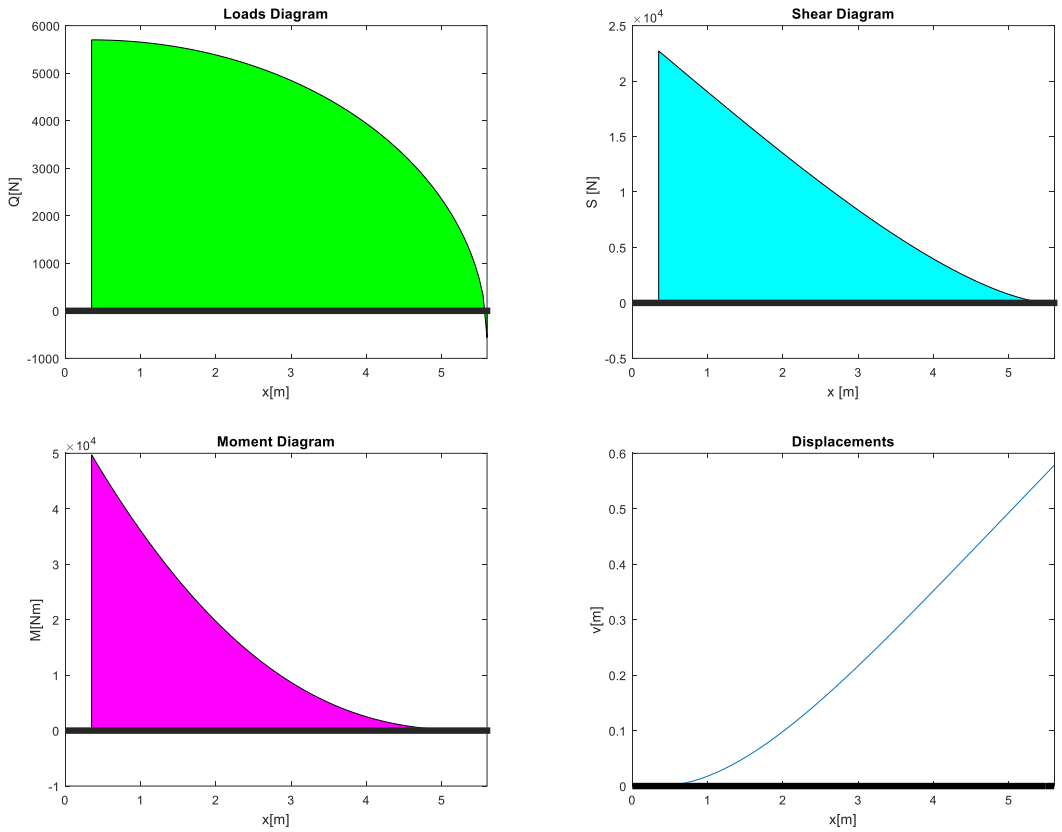

Figure 44. Main Wing Pre-sizing Results.

5.2.2 Front Wing Sizing & Tail Sizing

The same process that has previously been carried out to size the main malfunction is then applied to size the front wing and tail. The materials used, as well as the wing structure, are the same.

Following tables collect the results of the front wing and tail. It is thus observed that the most critical conditions remain the same as before.

Front Wing Pre-sizing Parameters			
Parameter	Symbol	Unit	Value
Max. Take-off Weight (15%)	$MTOW$	kg	175.5
Mean Geometric Chord	MGC	m	0.35
Wing Surface	S_W	m^2	1.53
Airfoil Thickness	t_{airf}	%	14
Wingspan	B_w	m	4.40
Reference Moment Coefficient	$C_{m_{ref}}$	-	-0.40
Security Factor	FS	-	3
Wide Spar Cap	w_{cap}	m	0.03
Estimated Cap Thickness	t_{cap}	m	0.02
Load Factor	n	-	6

Table 8. Front Wing Pre-sizing Parameters.

Front Wing Sizing Results			
Parameter	Skin Thickness [mm]	Shear Web Thickness [mm]	Tip Vertical Displacement [mm]
Speed: 250 Kts n: +6 G	2.26	4.79	80
Speed: 250 Kts n: -3 G	2.26	2.40	-40
Speed: 70 Kts n: +1.5 G	0.17	1.19	15
Speed: 100 Kts n: -1 G	0.33	0.79	-10

Table 9. Front Wing Sizing Results.

Tail Wing Pre-sizing Parameters			
Parameter	Symbol	Unit	Value
Max. Take-off Weight (10%)	$MTOW$	kg	117
Mean Geometric Chord	MGC	m	0.50
Wing Surface	S_W	m^2	5.30
Airfoil Thickness	t_{airf}	%	8
Wingspan	B_w	m	2.40
Reference Moment Coefficient	$C_{m_{ref}}$	-	-0.01
Security Factor	FS	-	3
Wide Spar Cap	w_{cap}	m	0.045
Estimated Cap Thickness	t_{cap}	m	0.02
Load Factor	n	-	6

Table 10. Tail Pre-sizing Parameters.

Front Wing Sizing Results			
Parameter	Skin Thickness [mm]	Shear Web Thickness [mm]	Tip Vertical Displacement [mm]
Speed: 250 Kts n: +6 G	0.24	3.91	13
Speed: 250 Kts n: -3 G	0.24	1.95	-7
Speed: 70 Kts n: +1.5 G	0.018	0.98	3
Speed: 100 Kts n: -1 G	0.04	0.65	-2

Table 11. Front Wing Sizing Results.

5.3 FINITE ELEMENT ANALYSIS

Composite materials are non-isotropic materials that have different behaviors depending on the orientation of the fibers and applied loads.

When simulating a composite material, different types of studies can be carried out depending on the purpose and the object of study of the same, and depending on the scale at which you are working.

As shown in Figure 45, there are three types of studios in finite elements on composite materials.

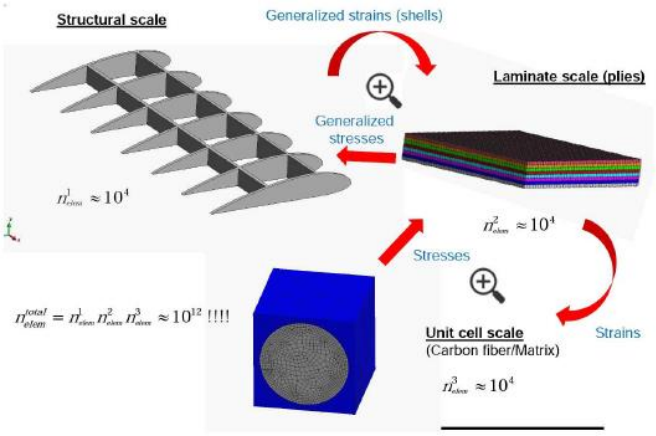

Figure 45. Composite Analysis Scales. Extracted from [19].

In essence, there is the so-called unit cell, which consists in evaluating the behavior of a single reinforcing fiber inside a cubic cell of resin. This type of studies is carried out when parameterizing the behavior of the compound at a micro scale, studying how it reacts against the different types of loads.

When several unit cells are joined, the study scale can be raised to the level known as the laminate scale. In this type of studies it is intended to find homogenized properties of the study material in order to be able to apply these properties to a structure, being able to analyze their real behavior.

As the computational cost of performing simulations in composite materials is very high, in order to carry out the studies in this thesis, the analysis performed are based in structural scale.

The homogenized properties have been extracted from the reference [21], which is a study that the author of the document carried out within the subject "Composite Materials" taught within the master itself.

Thus, the properties of the materials used can be seen in the following table.

Homogenized Materials' Mechanical Properties				
Parameter	**Units**	**Carbon Fiber + Epoxy**	**Glass Fiber + Epoxy**	**Foam (Isotropic)**
Longitudinal Young Modulus	MPa	91820	35000	60
Transverse Young Modulus	MPa	91820	9000	-
Normal Young Modulus	MPa	9000	9000	-
Poisson Ratio in XY Plane	-	0.05	0.28	0.3
Poisson Ratio in XZ Plane	-	0.3	0.28	-
Poisson Ratio in YZ Plane	-	0.3	0.4	-
Shear Modulus in XY Plane	MPa	19500	4700	-
Shear Modulus in XZ Plane	MPa	3000	4700	-
Shear Modulus in YZ Plane	MPa	3000	3500	-
Density	kg/m^3	1560	1770	81
Longitudinal Thermal Expansion	K^{-1}	2.5e-6	5.5e-6	0
Transverse Thermal Expansion	K^{-1}	2.5e-6	2.5e-5	-

Normal Thermal Expansion	K^{-1}	1.0e-5	2.5e-5	-
Longitudinal Tensile Stress	MPa	829	780	60
Longitudinal Compressive Stress	MPa	-439	-480	-
Transverse Tensile Stress	MPa	829	31	-
Transverse Compressive Stress	MPa	-829	-100	-
Shear Stress Limit in XY Plane	MPa	120	60	-
Shear Stress Limit in XZ Plane	MPa	50	60	-
Shear Stress Limit in YZ Plane	MPa	50	35	-

Table 12 Homogenized Material's Mechanical Properties.

5.3.1 Main Wing Analysis

By means of the Generative Structural Analysis module of CATIA V5 and the shell model developed in section 3.2, analyses of the wing under static load has been carried out in the most extreme conditions calculated previously.

Static load analysis is one of the most demanding because the structure is subjected to a load much higher than the one that can really undergo during the flight.

This first analysis is used to evaluate the conceptual design of the structure and thus have more or less accurate data to work with in order to optimize the structure and be able to carry out the detailed design of the aircraft.

The mesh that has been carried out meets high computational requirements, since a $20\ mm$ mesh with a $1\ mm$ sag has been calculated. The computational requirement is high because the size of the structure is very large compared to the size of the cell, which means that the number of operations to be performed is of the order of millions.

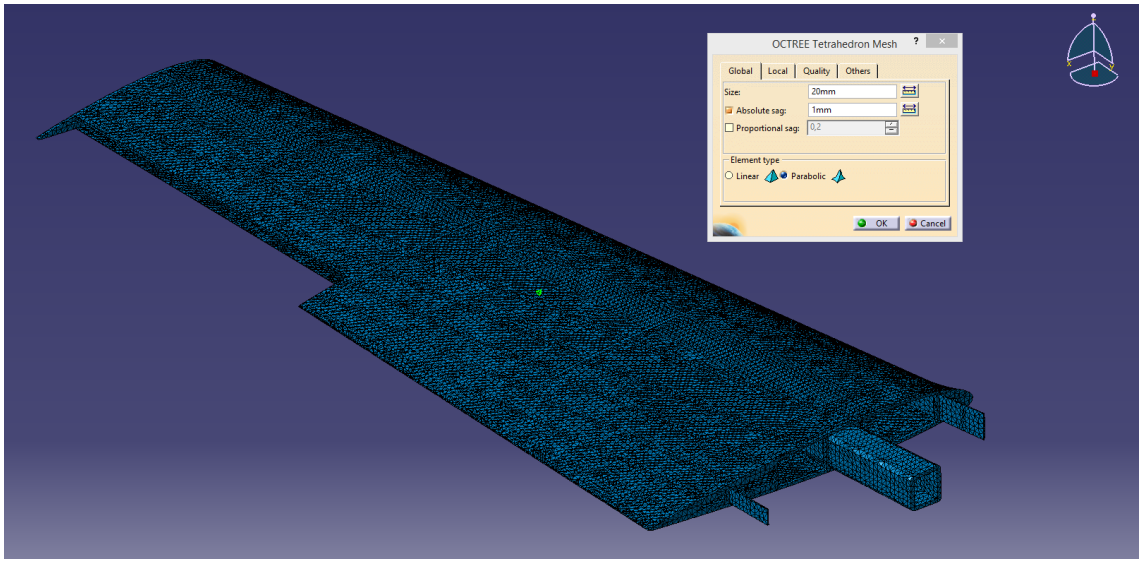

Figure 46. Main Wing Mesh.

As an anchoring point for the first analysis, a restriction of 6 degrees of freedom has been chosen for the spar and the stringers that protrude from the structure of the wing. This pretends to simulate the union of the wing with the fuselage.

On the other hand, a load has been distributed uniformly in the area marked in orange in Figure 47. This load is equivalent to 75% of the total lift obtained by flying at 250 kts and 6 G.

In turn, a load has been applied along the X-axis that simulates the drag in these conditions. This drag has been calculated using the polar curve calculated in the aerodynamics section,

$$L = 25825\ N \tag{26}$$

$$D = 3705\ N \tag{27}$$

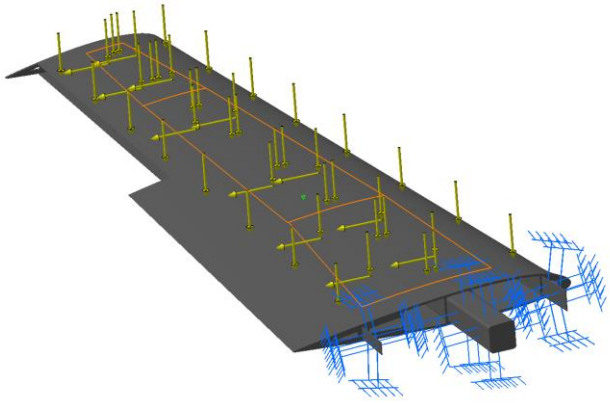

Figure 47. Wing Boundary Conditions.

As shown in figures 48, 49 and 50 the results obtained indicate that the wing bears the extreme conditions that have been imposed.

On the one hand, it can be observed how the maximum Von Misses Stress obtained is $500\ MPa$ and it is placed on the central spar below the first rib. This point where the tensions are concentrated, has a calculated safety factor of 1.65, higher than the minimum required by the 1.5 standard.

On the other hand it can be seen that the vertical displacement of the tip is $148\ mm$, much lower than that calculated in the pre-sizing phase.

Finally, it can be observed how there is tension concentration on the skin at those points where it joins with the ribs.

For a more detailed design of the structure, the author of the study proposes that the thickness of the skin be increased at said points to provide greater structural strength to the whole.

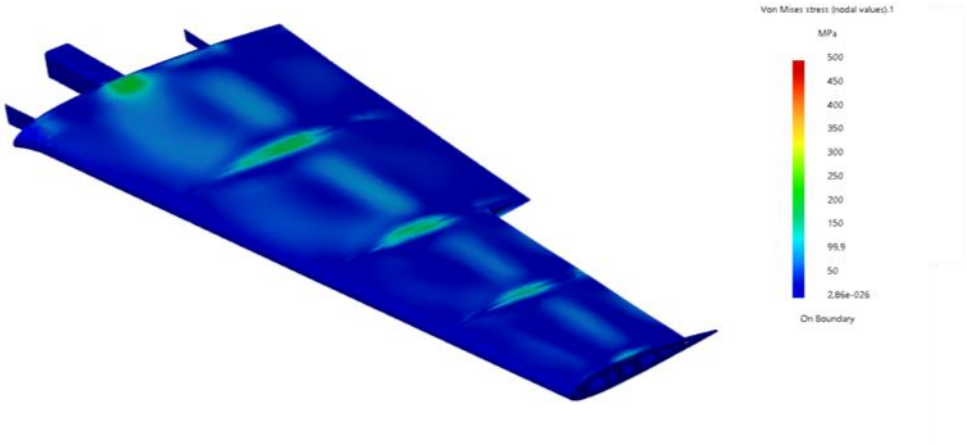

Figure 48. Von Misses Stress over skin.

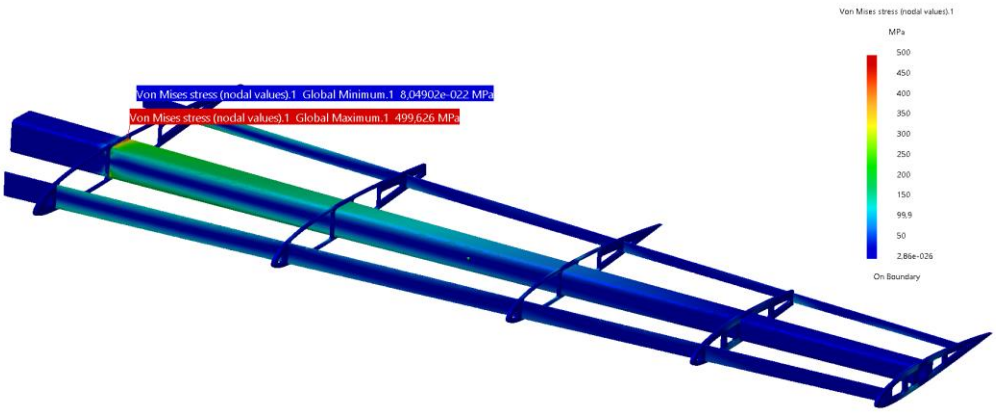

Figure 49. Von Misses Stress over the internal structure.

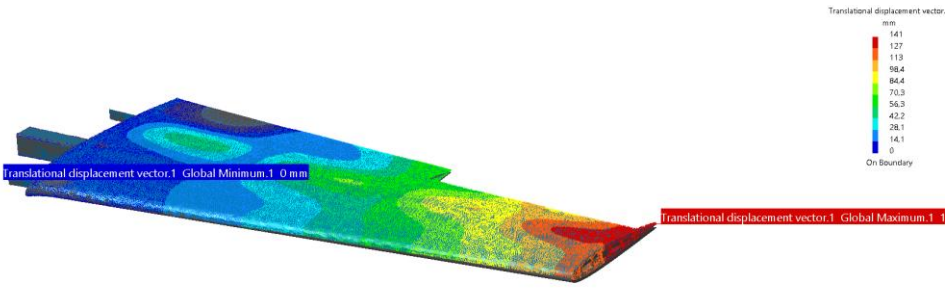

Figure 50. Wing Displacements.

5.3.2 Tail Analysis

The analysis of the tail has been carried out maintaining the same characteristics as in the previous analysis, both mesh and loading conditions.

For the case in question, a load has been distributed on the external surface of the tail, generating a torque around the X-axis. That is, for the right half-shell a positive lift has been produced with a value equivalent to the lift at $250\ kts.$ and $6\ G$, and for the left side a negative lift with the same value. In addition, the drag has been added.

$$L = \pm 3443\ N \tag{28}$$

$$D = 1324\ N \tag{29}$$

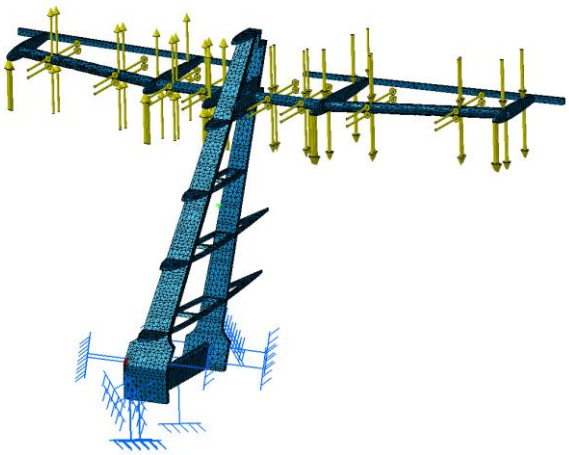

Figure 51. Tail Mesh and Boundary Conditions.

The results observed in Figure 52 show that there are two critical points of the structure, which are the joint of the tail and the arrow change in the front tube.

In these two points the value of the Von Misses voltage is $694\ MPa$, which equals a safety factor of 1.21. This value of the safety factor is lower than the 1.50 required by the regulations, so the design of the structure should be revised in future iterations.

A proposal to solve this problem would be to add more layers of fiber in those points or replace the tube with one with a wider thickness.

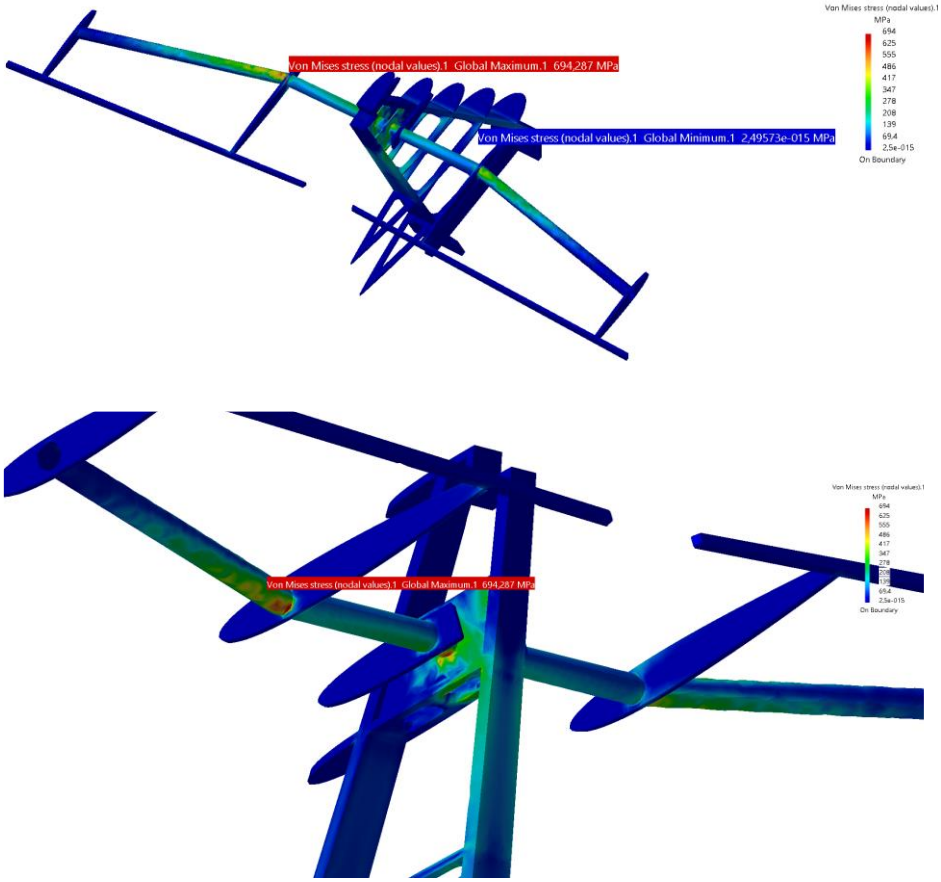

Figure 52. Von Misses Stress over Tail.

6. PERFORMANCE STUDIES

6.1 WEIGHT AND BALANCE

In the following section the estimation of the overall weight of the structure is exposed and a preliminary study is carried out to obtain the CG - Envelope chart. To perform these actions, the estimates and procedures shown in reference [2] and [22] have been followed.

The first step to determine the weight of the aircraft and calculate its CG is to define a coordinate system that is used to reference the position of the different components. In Figure 53, said reference system is shown.

As can be seen, the origin of coordinates is located in the nose of the plane. The X-axis takes the direction from nose to tail, the Y-axis follows the direction of the wing of the plane with positive direction towards the right point and the Z-axis takes the vertical direction.

The chosen coordinate system has these characteristics since it is the reference system used by the XFLR5 program and that has been transferred to CATIA V5. In this way, and with a common reference system, the design process is facilitated when carrying out the different iterations.

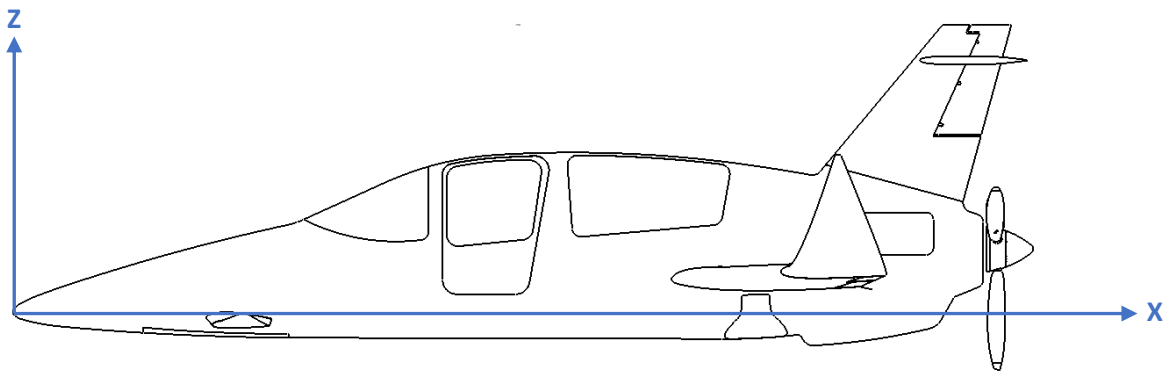

Figure 53. Aircraft Reference System

6.1.1 Weight Estimation

The estimation of the global weight of the aircraft has been carried out through a combination between the estimation of the components designed in CAD and the two semi-analytical estimation methodologies developed by the engineers D. P. Raymer and L.M. Nicolai, which are applied in those components that have not been designed.

In those components in which the approximations of D. P. Raymer and L. M. Nicolai are notably different, it has been decided to use an arithmetic mean to obtain the weight estimation.

The following table shows the input data that has been used to carry out the calculations of the weights of the non-designed components.

Weight Estimation Inputs			
Parameter	**Symbol**	**International System**	**Imperial System**
Total Fuel Quantity	Q_{tot}	280 L	74 gal
Fuel Quantity in Integral Fuel Tanks	Q_{int}	280 L	74 gal
Number of Tanks	N_{tank}	3	3
Number of Engines	N_{eng}	1	1
Number of Occupants	N_{occ}	4	4
Number of Crew	N_{crew}	2	2
Length of Fuselage Structure	L_{FS}	6847 mm	22.5 ft
Length of the Main Landing Gear Sturt	L_m	790 mm	31 in
Wingspan	B_W	10500 mm	34.5 ft
Ultimate Load Factor	n_l	6	6
Maximum Take-off Weight	W_o	1170 kg	2579 lb
Weight of unmounted avionics	W_{AV}	5 kg	11 lb
Weight of the Engine	W_{eng}	140 kg	257 lb
Mach Number	M	0.258	0.258
Dynamic Pressure	q_h	4636 Pa	97 lb/ft^2

Table 13. Weight Estimation Inputs

The estimates of the components not designed in CATIA V5 are shown below.

Landing Gear

Raymer
$$W_{MLG} = 0.095(n_l W_o)^{0.768}\left(\frac{L_m}{12}\right)^{0.409} = 231\ lb = 105\ kg \quad (30)$$

Nicolai
$$W_{MLG} = 0.054(n_l W_o)^{0.684}\left(\frac{L_m}{12}\right)^{0.601} = 70\ lb = 32\ kg \quad (31)$$

Average $W_{MLG} = 68.5\ kg$

Fuel system

Raymer
$$W_{FS} = 2.49 Q_{tot}^{0.726}\left(\frac{Q_{tot}}{Q_{tot}+Q_{int}}\right)^{0.363} N_{tank}^{0.242} N_{eng}^{0.157} = 57.5\ lb = 26\ kg \quad (32)$$

Nicolai
$$W_{FS} = 2.49\left[Q_{tot}^{0.6}\left(\frac{Q_{tot}}{Q_{tot}+Q_{int}}\right)^{0.3} N_{tank}^{0.2} N_{eng}^{0.13}\right]^{1.21} = 57.5\ lb = 26\ kg \quad (33)$$

Average $W_{FS} = 26\ kg$

Control system

Raymer $W_{CTRL} = 0.053 L_{FS}^{1.536} B_W^{0.371}(n_l W_o \cdot 10^{-4})^{0.8} = 33\ lb = 15\ kg$ (34)

Nicolai $W_{CTRL} = 1.066 W_o^{0.626} = 66\ kg$ (35)

Average $W_{CTRL} = 40.5\ kg$

Mounted avionics

Raymer $W_{AV} = 2.117 W_{UAV}^{0.933} = 20\ lb = 9\ kg$ (36)

Nicolai $W_{AV} = 2.117 W_{UAV}^{0.933} = 20\ lb = 9\ kg$ (37)

Average $W_{AV} = 9\ kg$

Electrical system

Raymer $W_{EL} = 12.57(W_{FS} + W_{AV})^{0.51} = 115.5\ lb = 52\ kg$ (38)

Nicolai $W_{EL} = 12.57(W_{FS} + W_{AV})^{0.51} = 115.5\ lb = 52\ kg$ (39)

Average $W_{EL} = 52\ kg$

Hydraulic system

Raymer $W_{HYD} = 0.001W_o = 2.6\ lb = 1\ kg$ (40)

Nicolai $W_{HYD} = 0.001W_o = 2.6\ lb = 1\ kg$ (41)

Average $W_{HYD} = 1kg$

Furnishings

Raymer $W_F = 0.0582W_o - 65 = 85\ lb = 39.5\ kg$ (42)

Nicolai $W_F = 34.5N_{crew}q_h^{0.25} = 216\ lb = 98\ kg$ (43)

Average $W_F = 69\ kg$

The table below shows the empty weight of the airplane taking into account the previously calculated estimates and the values obtained from the CAD design.

Component	Weight [kg]	X_{cg} [mm]	Y_{cg} [mm]	Z_{cg} [mm]	Determined by
Main Wing	112	5455	0	434	CAD
Canard	10	1591	0	112	CAD
Tail and Fuselage	118	4264	0	428	CAD
Landing Gear	68.5	2764	0	205	Estimation & CAD
Engine	140	6200	0	600	Technical Sheets
Fuel System	26	5243	0	420	Estimation & CAD
Control System	40.5	5243	0	420	Estimation & CAD
Mounted Avionics	9	2409	0	775	Estimation & CAD
Electrical System	52	2417	0	600	Estimation & CAD
Hydraulic System	1	2764	0	205	Estimation & CAD
Furnishings	69	3690	0	460	Estimation & CAD
Empty Aircraft	646	4492	0	463	Estimation

Table 14. Aircraft weights and centers of gravity. All the CG positions have been obtained from the CAD representation.

6.1.2 CG - Envelope

The CG - Envelope chart provides key information for the pilot when loading and distributing the weight, both passage and fuel.

For this reason, the author of the project considered it appropriate to calculate this envelope and whether to perform a first iteration of the calculation of static and dynamic stability, which are merely a reflection of the behavior and maneuverability of the aircraft.

The calculation of the flight envelope is made following the steps established in the EASA form of reference [23]. Although this form is designated for aircraft under the CS-LSA category, the procedure is valid for aircraft that are certified under CS-23.

6.1.3 Loading Cases

The following table shows the different components that confer the airplane, including weight and fuel. These components are used to calculate the aircraft's center of gravity for different flight configurations and obtain the limit curve.

Weight Items					
Item	Includes	Weight [kg]		X_{cg} [mm]	Determined by
Empty aircraft (W_{EW})	equipment and all necessary fluids (oil, coolant) except fuel	673		4492	Estimation
Fuel	unusable fuel	min 11	max 224	5243	Regulations
Pilot		min 55	max 100	3065	Regulations
Co-Pilot		min 0	max 100	3065	Regulations
Left Passenger		min 0	max 100	4310	Regulation
Right Passenger		min 0	max 100	4310	Regulations

Table 15. Aircraft Weight Items. It is used the table format of reference

The first step is to calculate the basic empty weight of the plane. This weight represents the empty weight of the aircraft next to the unusable fuel. This fraction of the fuel is usually between 5 and 10% of the total fuel of the aircraft [23].

It has been estimated, then, that the basic empty weight of the ODYSSEUS II that is being studied is of,

$$W_{BEW} = 684\ kg \tag{44}$$

The maximum empty weight is defined as the weight of the empty plane loaded with an $86\ kg$ pilot and with enough fuel to fly at a maximum speed of V_h for one hour.

Taking into account the fuel consumption of the engine according to the manufacturer is approximately $42\ L/h$, it is therefore considered that the fuel consumption needed to fly for one hour is $42\ L$ or $34\ kg$. Thus, the maximum empty weight is of,

$$W_{MEW} = W_{BEW} + W_{pilot} + W_{\min F} = 684 + 86 + 34 = 804\ kg \tag{45}$$

The minimum flying weight is that which simulates the weight of the airplane under the maximum load factor entering in a burst and taking into account that the pilot weights $55\ kg$.

$$W_{minFF} = W_{BEW} + W_{minpilot} = 684 + 55 = 739\ kg \tag{46}$$

The maximum weight of zero wing fuel weight is that which takes into account the empty basic weight plus the weight of the pilot and passengers, as well as unused fuel.

$$W_{MZF} = W_{BEW} + W_{maxpilot} + W_{maxpax} = 684 + 200 + 200 = 1084\ kg \tag{47}$$

The maximum takeoff weight of the aircraft determined by customer requirements is,

$$W_{MTOW} = 1170\ kg \tag{48}$$

The following table shows the different weights of the airplane that make up different combinations of situations and their respective centers of gravity calculated from the equation 48.

As can be seen, the positions fwd and aft of the maximum calculation take of weight are those calculated by XFLR5 in the static stability section (Figure 32).

Aircraft Weights						
		Includes		Centre of gravity		Requirement
Basic Empty weight	W_{BEW}	all necessary fluids (oil, coolant) and unusable fuel	684 kg	5041 mm		4.2.3 (AST)
Minimum flying weight	W_{min}	min pilot and unusable fuel	729 kg	4894 mm		4.2.2 (AST)
Minimum flying weight with full fuel	W_{minFF}	min pilot and full fuel	952 kg	4972 mm		Load calculation (EAS)
Maximum zero wing-fuel weight	W_{ZWF}	full useful load of W_{load}	1084 kg	4542 mm		5.2.1.3 (AST)
Maximum take-off weight	W_{MTOW}	combination of fuel and passenger load	1170 kg	fwd 4400 mm	aft 4700 mm	CS-LSA.5

Table 16. Loading Cases. Ref. [23]

$$X_{cg} = \frac{\sum W_i \cdot X_{cgi}}{\sum W_i} \tag{49}$$

6.1.4 Center of gravity locations

The CG of the aircraft is determined following the methodology described in the reference [23] and takes into account the results obtained in section 4.4.2 (Static stability study).These limits are,

- Most forward $4300\ mm$
- Most aft $4700\ mm$

The limited conditions that are studied below have been calculated based on the weight predictions in section 6.1.3 and the estimation of the position of the center of gravity obtained by the CAD design and the equation 49.

These conditions take into account different stages of the use of the airplane, since they take into account the airplane in flight and the operations on the ground.

As can be seen in graph 54, which represents the flight envelope, all the calculated combinations are located within the theoretical envelope. Except one.

Those situations in which the load of the plane is located inside the envelope, are safe situations, because the plane is stable within the limits explained during the aerodynamic analysis.

In the event of an aircraft's CG being too far forward, the maneuverability is compromised in the sense that a higher approach speed is required. With an excessive aft CG, it becomes an outright dangerous aircraft, since any low speed flight becomes most of the time unrecoverable. A guaranteed accident.

However, and as a comment for future studies, this point should be thoroughly reviewed and calculated in more detail if the plane is stable under such conditions.

	Condition	Pilots [kg]		Fuel [kg]		Passengers [kg]		Aircraft weight [kg]	Aircraft CG [mm]
CG envelope limits for flight	$W_{MTOW,aft}$		73	Max	224	Max	200	1170	4830
	$W_{MTOW,fwd}$	Max	200		111	Max	200	1170	4328
	$W_{min,aft}$	Min	55	Min	11	Min	0	729	4436
	$W_{min,fwd}$	Min	55	Min	11	Min	0	729	4436
Loading conditions in flight	W_{minFF}	Min	55	Max	224	Min	0	952	4572
	$W_{ZWF,aft}$	Max	200	Min	11	Max	200	1074	4227
	$W_{ZWF,fwd}$	Max	200	Min	11	Min	0	874	4208
	$W_{minFFbag}$	Min	55	Max	224	Max	200	1142	4564
Loading conditions on ground	W_{BEW}		0	Min	11	0	0	674	4548
	W_{aftmax}		0	Min	11	Max	200	874	4493

Table 17. Loading Cases on center of gravity envelope for standard configuration. Ref. [18].

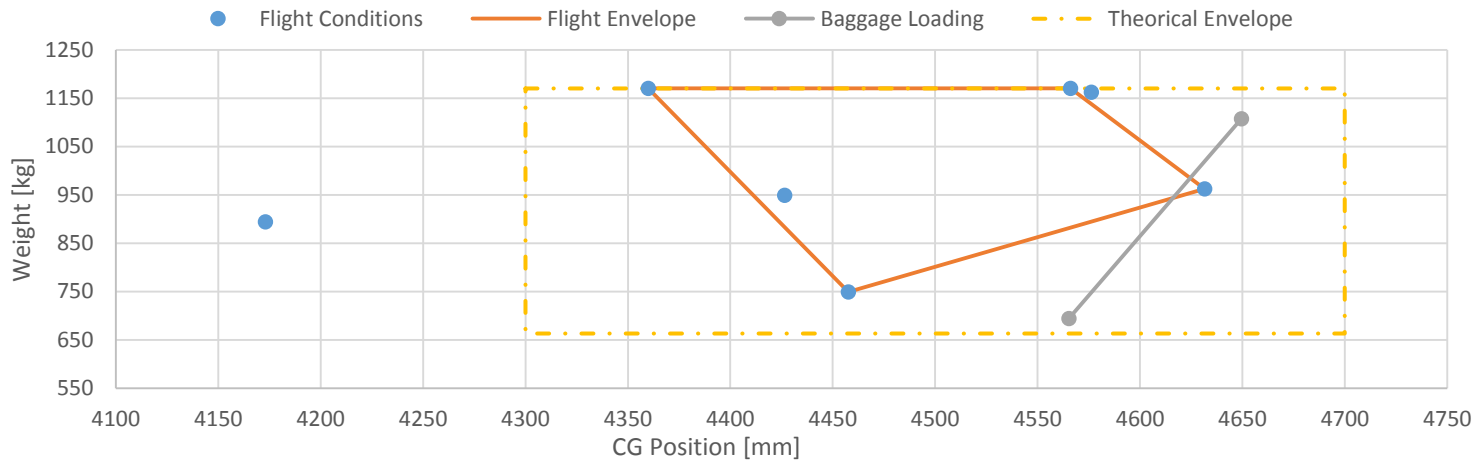

Figure 54. CG-Envelope

6.2 RANGE ESTIMATION

The range has been estimated through the code of the Annex 10.3 that applies the Breguet equation, using the methodologies established in the references [2] and [24]. This code was developed by the author of the thesis in the framework of his final degree thesis.

$$Range = \frac{V}{g} \cdot \frac{L}{D} \cdot \frac{1}{SFC} \cdot \eta_p \cdot \ln\left(\frac{W_{in}}{W_f}\right) \tag{50}$$

Where SFC is defined as the mass flow rate of fuel per unit of thrust in $(Kg/s/N)$, and η_p is the propeller efficiency.

The calculations have been done using the nominated cruise speed $(170\ kts)$ seen in the requirements of the thesis.

Other considerations for this estimation is that the total fuel reserve is a 10% of the total fuel that can carry the airplane, which is translated in $25\ kg$,

The specific fuel consumption is calculated from the cruise power (around 60% of the total engine power), and for conservative reasons the propeller efficiency is around 40%.

$$T_{cruise} = \frac{P_{cruise}}{V_{cruise}} \tag{51}$$

$$SFC_{cruise} = \frac{FC_{cruise}}{T_{cruise}} \tag{52}$$

Figure 55 shows the payload rage diagram calculated for the ODYSSEUS II plane. As it is observed, the maximum payload weight that the airplane could carry, counting passage and equipage, is of $262\ kg$.

With the airplane fully loaded, it is possible to fly $2200\ km$ (red circle in Figure 56). As the payload weight decreases it is possible to increase the range up to $2750\ km$ (blue circle).

The results of this analysis meet the requirement of having a range of 6.5 hours, without counting the reserve fuel. 6.5 hours at a speed of 170 kts make a range of 2047 km. Thus, the plane meets the requirements of the designer.

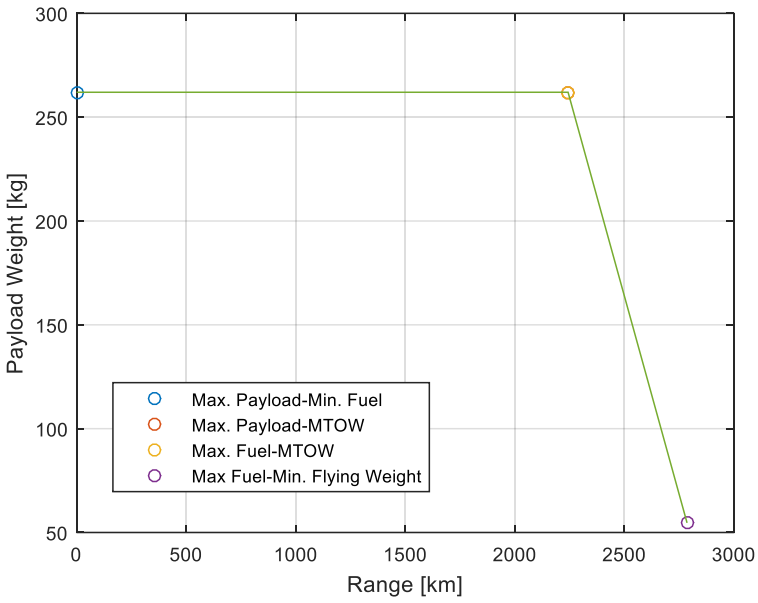

Figure 55. Payload-Range Diagram

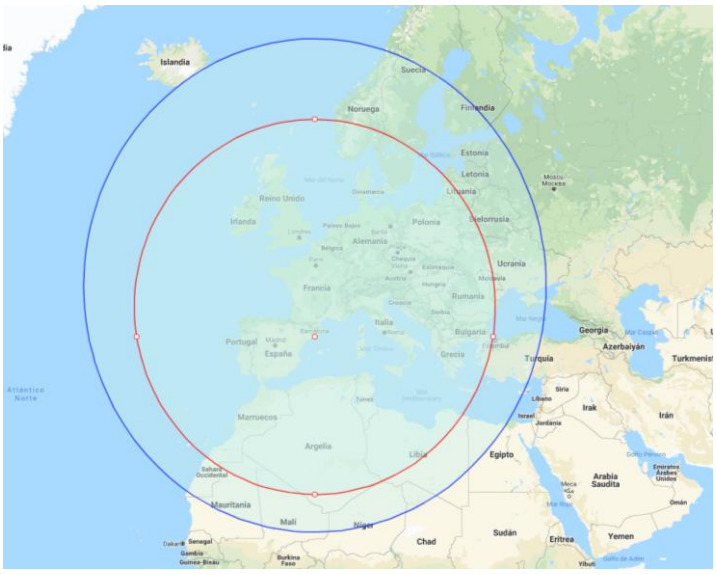

Figure 56. ODYSSEUS II Range over Europe

7. CONCLUSIONS

7.1 AERODYNAMIC CONCLUSIONS

In the field of aerodynamics it has been seen that the solution designed by Marc Kuster is viable and safe. Its commitment to a three-surface aircraft design allows the behavior of the ODYSSEUS II to be secure and maneuverable.

One of the strengths of this design is the low stall speed thanks to the extra lift achieved with the use of a canard.

Despite some difficulty in finding the CG range to ensure stability, it is noteworthy that the ODYSSEUS II is within normal stability limits.

After studying the design in more details, it can be concluded that the ODYSSEUS II drag is a little higher than that of a conventional airplane with similar characteristics. This factor, caused by the added surface of the elevator wing, also affects the aircraft's aerodynamic efficiency, which, as seen in the theoretical exposé, is usually less than that of a similar aircraft.

Therefore, in view of the studies carried out and in the absence of studying more carefully the design of flaps and control surfaces, the author of this thesis states that the aerodynamic design meets the requirements proposed by the designer and current regulation

7.2 STRUCTURAL CONCLUSIONS

After studying the different existing structural options, a monocoque structure design is proposed for ODYSSEUS II.

The analysis of this structure shows that both wings and tail structure are safe within the most extreme conditions of the flight envelope limits as well as complying with all regulations.

Apart from these results, it must be noted that tail structure should be redesigned as the safety factor does not meet the 1.5 safety factor for conformance.

As a result, the author concludes that it is necessary to carry out more analyzes on the entire structure of the aircraft, before starting with the detailed designs.

However, the results in general, including the aerodynamics, are good enough to continue with the project proposed by the designer.

7.3 PERFORMANCE CONCLUSIONS

In the performance section, the CG centering of the aircraft and the range have been evaluated. It has been seen that the aircraft is well centered in all cases imposed by the standards, except for one.

Given this, and based on the future structural changes that must be made, the centering of the aircraft must be recalculated to confirm that all the planned points meet the requirements.

The calculations are promising and validate the continuation with this design.

Finally, regarding the range, it has been seen that using the engine proposed by the designer and the data calculated in the different sections of the thesis, the maximum range of the aircraft meets the minimum requested by Mr. Kuster.

In conversations with the designer, the possibility of replacing the combustion engine with an electric motor of similar characteristics appeared. An option that, in the eyes of the thesis author, is entirely valid. This substitution will imply recalculating the range to make sure that the requirement continues to be met.

7.4 THESIS CONCLUSIONS

As conclusions of the thesis, on a personal basis, the author of the project is strongly satisfied with the results, since he has been able to carry out the study of an aircraft in the design phase, and which is intended to be built.

On the other hand, the author has been able to carry out a consultant / engineer role that serves a client with a need. This has been a pleasant experience which I would not hesitate to repeat.

7.5 FURTHER WORK

As future short-term works, the author of this thesis believes that it is necessary to conduct more studies on the aerodynamic design, as well as more detailed analysis on specific elements such as flaps, control surfaces and winglets.

The process of these further studies can be performed in the same manner as those presented in this thesis.

With respect to the structural field, the author proposes more exhaustive studies to be carried out such components as the landing gear, the fuselage and canard.

At the same time, a full study of aerolasticity would be convenient, in order to provide greater design security before the start of construction.

In the long term, the author proposes the fabrication of sample specimens of the materials intended to be used, including laboratory testings.

Finally, the ODYSSEUS II will be required to pass several non-destructive tests to prove its safety and reliability.

As for the study of performance, further factors should be studied, such as maximum speed, landing and take-off distances, climb speed and other maneuvers.

8. REFERENCES

[1] EAA. *Experimental Amateur-Built Aircraft Sourcebook.* EAA. 2018 [Online] https://www.eaa.org/~/media/files/eaa/homebuilders/EAA_ExpAmatuerBuildSourcebook

[2] Gudmunsson S. *General Aviation Aircraft Design: Applied Methods and Procedures.* First Edition. Elsevier. 2014

[3] FAA. *Aviation Maintenance Technician Handbook-Airframe, Volume 1*. FAA. 2018 [Online] https://www.faa.gov/regulations_policies/handbooks_manuals/aircraft/media/amt_airFrame_hb_vol_1.pdf

[4] Raymer D. *Aircraft Design: A conceptual Approach*. AIAA. Fifth Edition 2012

[5] Dassault Systemes. *CATIA V5*. 3DS. 2019. [Online] https://www.3ds.com/es/productos-y-servicios/catia/

[6] Horne Thomas A. *Stemme S10-VT: Powersailing*. AOPA. 2014. [Online] https://www.aopa.org/news-and-media/all-news/2014/november/pilot/f_stemme

[7] Domun Y. *Aircraft Design Process Overview*. Engineeringclicks. 2016 [Online] https://www.engineeringclicks.com/aircraft-design-process/

[8] Amadori K. *On Aircraft Conceptual Design*. Linköping University. 2008.

[9] Reed J. A. *Improving the aircraft design process using Web-based modeling and simulation.* ACM Trans. Model. Comput. Simul. 2000

[10] Gudmunsson S. *APP2: Design of Canard Aircraft*. Elsevier. 2014

[11] Anon. *Canard Efficiency Myths.* Apollo Canard. 2012 [Online] http://www.apollocanard.com/4_canard%20myths.htm

[12] Airfoiltools. 2019 [Online] http://airfoiltools.com/

[13] Torenbeek E. *Synthesis of subsonic airplane design*. Delf University. 1976.

[14] XFLR5. *XFLR5 Documentation*. XFLR5. 2019 [Online] http://www.xflr5.com/xflr5.htm

[15] Campos D. *Project of a new LSA semi-aerobatic airplane*. ESEIAAT. 2017

[16] Sadrey M. *Aircraft Performance Analysis*. 2009

[17] EASA. *CS23 Amendment 3*. EASA

[18] Hernández J. *Mechanics of unidirectional ply*. ESEIAAT. 2018

[19] Doherty D. *Analytical Modeling of Aircraft Wing Loads Using MATLAB and Symbolic Math Toolbox*. Mathworks. 2009. [Online]. https://es.mathworks.com/company/newsletters/articles/analytical-modeling-of-aircraft-wing-loads-using-matlab-and-symbolic-math-toolbox.html

[20] Gil L. *Estructures Aeroespacials*. UPC. 2016.

[21] Campos. D. *Assignment 3: Laminated composite plate*. ESEIAAT. 2018

[22] Shpati. G. *Aircraft CG Envelopes*. 2011 [Online] http://www.sawe.ca/download/tech2011/Aircraft%20CG%20Envelopes.pdf

[23] EASA. *ABCD-FE-01-00 Flight Envelope-v1 08.03.16*. EASA

[24] Anon. *Aircraft Performance and Flight Mechanics*. Clarkson University

[25] Anon. *Operation Reference Manual IO-390 Series*. Lycoming. 2018

9. BUDGET

The following is the budget of the study carried out in the framework of the thesis of the end of the master. This budget has been calculated in a detailed manner, as can be seen in the tables.

Hiring Fees				
Concept	**Responsibility**	**Hours**	**€/hour**	**Total €**
Project Management	Coordinator	38	70	2.660 €
Project Development	Developer	227	40	9.080 €
Software and Licencies	-	-	-	1.164 €
			Total	12.904 €

Table 18. Hiring Fees.

Study Development Detail				
Department	**Task**	**Hours**	**Total Hours**	**Total €**
Management	Requirements Study	4	38	2.660 €
	Scheduling	4		
	Coordination	10		
	Reporting	20		
Aerodynamics	Information Research	15	110	4.400 €
	Modelling	20		
	XFLR5 Analysis	25		
	CFD Analysis	50		
Structures	Information Research	15	100	4.000 €
	CAD Design	50		
	Structural Pre-sizing	15		
	Structural Analysis	20		
Performances	Information Research	5	17	680 €
	CG-Envelope	8		
	Range Study	4		
			Subtotal	11.740 €

Table 19. Study Development Details

Software and Licences		
Software	**Licence**	**Price €**
CATIA V5 R2017	Student	100
Ansys R17	Student	0
XFLR5	Open Source	0
Keyshot 6	HD Version	995
Matlab Student	Student	69
	Subtotal	1.164 €

Table 20. Software and Licences

10. ANNEXES

10.1 FLIGHT ENVELOPE CODE

```
%% FLIGHT ENVELOPE
clear all; clc;

% AIRCRAFT PARAMETERS
    MTOM  = 1170;
    g     = 9.81;
    MTOW  = g * MTOM;
    Sw    = 10;
    MGC   = 1.23;
    nmax  = 6;
    nmin  = -3;
    nmaxf = 2;
    nminf = 0;

    % Coefficients
    CLmax = 1.2;
    Clmax = 1.9;
    Clff  = 2.25;
    Clto  = 2.05;
    CLmin = -0.7;
    red   = CLmax/Clmax;
    CLff  = red * Clff;
    CLto  = red * Clto;
    a     = 4.97;

% FLIGTH CONDITIONS
    rho = 1.225;

% SPEEDS [KEAS]
    % Maximum Speed
    Vh = 250;

    % Stall Speeds
    Vs  = sqrt(2  * MTOW/(rho * CLmax * Sw))/0.5144;
    Vso = sqrt(2 * MTOW/(rho * CLff * Sw))/0.5144;
    Vs1 = sqrt(2 * MTOW/(rho * CLto * Sw))/0.5144;
    Vs2 = sqrt(2 * MTOW/(rho * abs(CLmin) * Sw))/0.5144;

    % Design Manoeuvring Speed
    Va    = Vs * sqrt(nmax);
    Vaneg = Vs2 * sqrt(abs(nmin));
    Vaf   = Vso * sqrt(nmaxf);

    % Flaps Speeds
    Vf  = 120;
    Vff = Vf;

    % Cruise, Dive and Never Exceed Speeds
    Vc  = 170;
```

```
    Vd  = 250;
    Vne = 250;

% GUST
    n3c = zeros(100,1);
    n3d = zeros(100,1);
    n4c = zeros(100,1);
    n4d = zeros(100,1);

    Udec = 15;
    Uded = 7.5;

    Vudec = linspace (0,Vc);
    Vuded = linspace (0,Vd);

    mug = 2 * MTOW/(rho * MGC * a * Sw);
    kg  = 0.88 * mug/(5.3 + mug);

    for i = 1:100
        n3c(i) = 1 + 0.5 * rho * kg * Vudec(i) * a * Udec/(MTOW/Sw)
* 0.5144;
        n3d(i) = 1 + 0.5 * rho * kg * Vuded(i) * a * Uded/(MTOW/Sw)
* 0.5144;
        n4c(i) = 1 - 0.5 * rho * kg * Vudec(i) * a * Udec/(MTOW/Sw)
* 0.5144;
        n4d(i) = 1 - 0.5 * rho * kg * Vuded(i) * a * Uded/(MTOW/Sw)
* 0.5144;
    end

    % PLOT
    seg1 = [Va Vd];
    seg2 = [Vd,Vd];
    seg3 = [Vaneg Vd];
    seg4 = [Vs2 Vs2];
    seg5 = [Vs Vs];
    seg6 = [Vaf Vff];
    seg7 = [Vso Vff];
    seg8 = [Vso Vso];
    seg9 = [Vff Vff];

    % Stall lines
    V    = linspace(Vs,Va);
    Vneg = linspace(Vs2,Vaneg);
    Vf   = linspace(Vso,Vaf);
    n    = zeros(100,1);
    nneg = zeros(100,1);
    nf   = zeros(100,1);

    for i = 1:100
        n(i)    = 0.5 * rho * V(i)^2 * Sw * CLmax/MTOW * 0.5144^2;
        nneg(i) = 0.5 * rho * Vneg(i)^2 * Sw * CLmin/MTOW *
0.5144^2;
        nf(i)   = 0.5 * rho * Vf(i)^2 * Sw * CLff/MTOW * 0.5144^2;
    end

    plot(seg1,[nmax nmax],'-k',...
```

```
        seg6,[nmaxf nmaxf],'-r',...
        Vudec,n3c, '--b',...
        seg2,[nmax nmin],'-k',...
        seg3,[nmin nmin],'-k',...
        seg4,[0 -1], '-k',...
        seg5,[0 1],'-k',...
        V,n,'-k',...
        Vneg,nneg,'-k',...
        seg7,[0 0],'-r',...
        Vf,nf,'-r',...
        seg8,[0 1],'-r',...
        seg9,[0 nmaxf],'-r',...
        Vuded,n3d,'--b',...
        [Vc Vd], [n3c(100) n3d(100)],'--b',...
        Vudec,n4c,'--b',...
        Vuded,n4d,'--b',...
        [Vc Vd],[n4c(100) n4d(100)],'--b');

    xlabel('Aispeed [KEAS]')
    ylabel('Load Factor')
    ylim([-5  7])
    xlim([0 260])


    legend('Manoeuvre Diagram', 'Flap Manoeuvre Diagram', 'Gust
Diagram')
grid on; grid minor;
```

10.2 STRUCTURE PRE-SIZING

```
%% WING STRUCTURE PRE-DESIGN
clc; clear all; close all;
% AIRCRAFT DATA
    % MTOW:  Maximum take-off weight [kg]
    % MF:    Fuel Mass [kg]
    % Sw:    Wing Surface [m^2]
    % Cmgc:  Mean Geometric Chord [m]
    % t_c:   Airfoil thickness [mm]
    % b:     Wingspan [m]
    % bf:    Fuel span [m]
    % Cmref: Reference moment coefficient
    % FS:    Security factor

    % Wing Spar
    MTOW  = 1170*0.10; % Kg
    MF    = 0;         % kg
    Sw    = 5.30;      % m^2
    Cmgc  = 0.50;       % m
    t_c   = 0.08;
    b     = 2.40;      % m
    bf    = 1.85;        % m
    Cmref = -0.01;
    FS    = 3;
    Sref  = Sw/2;       % m
    bref  = b/2;        % m

%     % Canard Spar
%     MTOW  = 15;      % Kg
%     MF    = 0;       % kg
%     Sw    = 1;        % m^2
%     Cmgc  = 0.47;      % m
%     t_c   = 0.11;
%     b     = 3.8;         % m
%     bf    = 0;         % m
%     Cmref = -0.4;
%     FS    = 1.5;
%     Sref  = Sw/2;      % m
%     bref  = 1.7; % m
%
% FLIGHT CONDITIONS
    % nmax: Flight Gs
    % rho:  Air density [kg/m^3]
    % V:    Speed [m/s]
    % g:    Gravity [kg/m^3]

    nmax = 6;
    rho  = 1.225; % kg/m^3
    V    = 130;   % m/s
    g    = 9.81;  % m/s^2

% MATERIALS PROPERTIES
    % Carbon Fiber + Epoxy
    % rhoc:   density of carbon fiber [kg/m^3]
    % sigmac: Ultimate Yield Tensile of carbon fiber [Pa]
    % Ec:     Young Modulus of carbon fiber [Pa]
```

```
    % tauc:   Ultimate Shear Tensile of carbon fiber [Pa]

    rhoc   = 1590;   % kg/m^3
    sigmac = 835e6;  % Pa
    Ec     = 67.6e9; % Pa
    tauc   = 97e6;   % Pa

    % Glass Fiber + Epoxy
    % rhog:   density of glass fiber [kg/m^3]
    % sigmag: Ultimate Yield Tensile of glass fiber [Pa]
    % Eg:     Young Modulus of glass fiber [Pa]
    % taug:   Ultimate Shear Tensile of glass fiber [Pa]

    rhog   = 1770;   % kg/m^3
    sigmag = 320e6;  % Pa
    Eg     = 24.8e9; % Pa
    taug   = 99e6;   % Pa

% THICKNESS OF THE SKIN
    % Skin Parameters
    E_skin   = Eg;
    rho_skin = rhog;
    tau_skin = taug/FS;

    % Torsion Load at Root
    Tor = 0.5 * rho * V^2 * Cmgc * Sref * Cmref;

    % Cell Characteristics
    Ccell = 0.65 * Cmgc;
    h     = Cmgc * t_c;
    Acell = 2/3 * Ccell * h;

    % Skin Thickness Computatuon
    t_skin = abs(Tor)/(2 * Acell * tau_skin);

    disp('Skin Thickness [mm]');
    disp(t_skin * 1000);

% THICKNESS OF SHEAR WEB
    % Web Parameters
    rho_web = rhog;
    tau_web = taug/FS;

    % Shear Load at Root
    V     = nmax * MTOW * g/2;
    t_web = 3/4 * nmax * g * MTOW/h/tau_web;

    disp('Shear Web Thickness [mm]')
    disp(t_web * 1000);

% THICKNESS OF THE WING SPAR CAPS
    % Caps Parameters
    w_cap   = 0.12;
    h_cap   = Cmgc * t_c - 2 * t_skin;
    t_cap   = 0.015;
```

```
    A_cap   = t_cap * w_cap * 2;
    rho_cap = rhoc;
    E_cap   = Ec;
    I_cap   = w_cap * h_cap^3/12 - w_cap * (h_cap -  2 *
t_cap)^3/12;


% ANALISYS PROPERTIES
    nel = 100;
    % GEOMETRY
    % nd: problem dimensions
    % nel: total bars
    % n: total number of nodes
    % ngle: elements degrees of freedom
    % ngl: total degrees of freedom
    % nnod: number of nodes in bar

    % x: node coordenades
    % T: connectivity table
    nd   = 1;
    n    = nel + 1 ;
    ngle = 2;
    ngl  = n * ngle ;
    nnod = 2;

    % Computation of X
    x = zeros(1,n);

    for i = 2:n
        x(i) = bref/nel * (i - 1);
    end

    % Computation of T and xfq
    T = zeros(2,nel);

    for i = 1:nel
        T(1,i) = i;
        T(2,i) = i + 1;
    end

% DISTRIBUTED AND PUNTUAL LOADS
    Q      = zeros(n,1);
    qf     = zeros (n,1);
    q_cap  = zeros (n,1);
    q_skin = zeros (n,1);
    q_web  = zeros (n,1);

    % Estimated Loads
    for i = 1:n
        ql         = 2 * MTOW * g * nmax * sqrt(bref^2 - x(i)^2)/(pi
* bref^2);
        q_cap(i)  = -rho_cap * A_cap * bref/nel;
        q_skin(i) = -2 * rho_skin * Sref * t_skin/nel;
        q_web(i)  = -rho_web * bref/nel;

        if x(i) >= 0.35 && x(i) <= bf + 0.35
```

```
            qf(i) = -MF * g/2/bf;
        end

        Q(i) = ql + nmax * (q_cap(i) + q_web(i) + q_skin(i) +
qf(i));
    end

% COMPUTATION OF ELEMENT STIFFNESS MATRICES AND DISTRIBUTED LOAD
    % le : bar longitude
    % x1e... : coordenades of the bar's nodes
    % Compute element matrix
    le   = zeros (nel,1);
    Kel  = zeros (nnod * ngle,nnod * ngle,nel);
    Fext = zeros (ngl,1);

    for e = 1:nel
        x1e   = x(1,T(1,e));
        x2e   = x(1,T(2,e));
        c1e   = T(1,e) * 2 - 1;
        c2e   = T(2,e) * 2 - 1;
        n1e   = T(1,e) * 2;
        n2e   = T(2,e) * 2;
        le(e) = x2e - x1e;
        Ke = (E_cap*I_cap/le(e)^3)*[12 6*le(e) -12
6*le(e);6*le(e)...
            4*le(e)^2 -6*le(e) 2*le(e)^2;-12 -6*le(e) 12 -
6*le(e);6*le(e)...
            2*le(e)^2 -6*le(e) 4*le(e)^2];

        % Distributed Load
        Fext(c1e) = Fext(c1e) + 1/2 * Q(e) * le(e);
        Fext(c2e) = Fext(c2e) + 1/2 * Q(e+1) * le(e);
        Fext(n1e) = Fext(n1e) + 1/bref * Q(e) * le(e)^2;
        Fext(n2e) = Fext(n2e) - 1/bref * Q(e+1) * le(e)^2;

        for i = 1:nel
            for r = 1: nnod*ngle
                for s = 1: nnod*ngle
                    Kel(r,s,e) = Ke(r,s);
                end
            end
        end
    end

% GLOBAL MATRIX
    KG = zeros(ngl, ngl);

    % Assembling of stiffness matrix
    for e = 1:nel
        for a = 1:nnod
            for i = 1:ngle
                r = ngle * (a-1) + i;
                A = T(a,e);
                p = ngle * (A-1) + i;

                for b = 1:nnod
```

```
                    for j = 1: ngle
                        s = ngle * (b-1) + j;
                        B = T(b,e);
                        q = ngle * (B-1) + j;

                        KG(p,q) = KG(p,q) + Kel(r,s,e);
                    end
                end
            end
        end

    end

    % Free Nodes
    vl = zeros(1,ngl-2);

    for i = 2:ngl-2
        vl(1) = 3;
        vl(i) = vl(i-1) + 1;
    end

    % Restricted Nodes
    vr  = [1 2];
    Kll = KG(vl,vl);
    Klr = KG(vl,vr);
    Krl = KG(vr,vl);
    Krr = KG(vr,vr);

    % Reduce global system
    ul(vl) = Kll\Fext(vl);

% REACTIONS
    r(vr) = Krl * ul(vl)' - Fext(vr);
    R     = zeros(ngl,1);

    for i = 1:2
        R(i) = r(i);
    end

    displ = reshape (ul,ngle,n);

    F = Fext + R;
    B = zeros (n,2);
    l = zeros(n,1);

    for i = 1:n
        l(i) = (i-1) * bref/nel;
        stop = 0;
        for j = 1:n
            if x(j) > l(i) && stop ==0
                n0   = j;
                stop = 1;
            end
        end
        for k = n0:n
```

```
            s = 2 * k-1;
            m = 2 * k;

            B(i,1) = B(i,1) + F(s);
            B(i,2) = B(i,2) + F(m) - F(s) * (l(i) - x(k));
        end
    end

% RESULTS
    disp('Tip Vertical displacement [m]')
    disp (displ(1,n));


% PLOTS
    viga = zeros(1,n);
    figure (1)
    h = area (x+0.35,Q);
    h.FaceColor = 'g';
    bl = h.BaseLine;
    bl.LineWidth = 5;
    xlim([0 bref+0.35]);
    xlabel('x[m]')
    ylabel('Q[N]')
    title('Loads Diagram')

    figure (2)
    h = area (x+0.35,B(:,1));
    h.FaceColor = 'c';
    bl = h.BaseLine;
    bl.LineWidth = 5;
    xlim([0 bref+0.35]);
    xlabel('x [m]')
    ylabel('S [N]')
    title('Shear Diagram')

    figure(3)
    plot(x,viga,'k','LineWidth',8);
    h = area (x+0.35,B(:,2));
    h.FaceColor = 'm';
    bl = h.BaseLine;
    bl.LineWidth = 5;
    xlim([0 bref+0.35]);
    xlabel('x[m]')
    ylabel('M[Nm]')
    title('Moment Diagram')

    figure(4)
    xd = linspace(0,bref+0.35,n);
    DISP = plot(x+0.35,displ(1,:));
    hold on;
    BEAM = plot(xd,viga,'k');
    set(BEAM,'LineWidth',5);
    xlabel('x[m]')
    ylabel('v[m]')
    xlim([0 bref+0.35]);
    title('Displacements')
```

10.3 PAYLOAD RANGE

```
%% PAYLOAD-RANGE DIAGRAM
clear all; clc; close all;

% AIRCRAFT PARAMETERS
% Cruise Conditions
    Vc = 170;          % KTS
    V  = Vc * 0.5144; % m/s
    Dc = 3500;         % N
    g  = 9.81;         % m/s^2

% Weights
    MTOW  = 1170;      % kg
    MZFW  = 946;       % kg
    OEW   = 684;       % kg
    MFW   = 224;       % kg
    RF    = 25;        % kg
    minPL = 55;        % kg

% Engine Parameters
    FC  = 42;              % L/h
    FC  = 0.8 * FC/3600 ; % kg/s
    P = 156000 * 0.6;      % W
    T = P/V;               % N
    SFC = FC/T;            % kg/s/N
    rhop = 0.4;

% POINT 1: MAX PAYLOAD-MIN FUEL
    MPL = MZFW - OEW;
    R = 0;

% POINT 2: MAX PAYLOAD-MTOW
    FW1 = MTOW - OEW - MPL - RF;
    LW1 = MTOW - FW1;
    E1  = ((MTOW+LW1)/2) * g/Dc;
    R1  = (V/SFC) * rhop * E1 * log(MTOW/LW1);

% POINT 3: MAX FUEL-MTOW
    PL2 = MTOW - MFW - OEW;
    LW2 = MTOW - MFW + RF;
    E2  = ((MTOW + LW2)/2) * g/Dc;
    R2  = (V/SFC) * rhop * E2 * log(MTOW/LW2);

% POINT 3: MAX FUEL-MinPL
    PL3 = minPL;
    TOW = OEW + MFW + PL3;
    LW3 = TOW - MFW + RF;
    E3  = ((MTOW + LW2)/2) * g/Dc;
    R3  = (V/SFC) * rhop * E3 * log(TOW/LW3);

    Range = [R R1 R2 R3]/1000;
    PL = [MPL MPL PL2 PL3];


plot(Range(1),PL(1),'o',Range(2),PL(2),'o',Range(3),PL(3),'o',...
```

```
    Range(4),PL(4),'o',Range,PL);
    grid on;

    xlabel ('Range [km]');
    ylabel ('Payload Weight [kg]');

    legend('Max. Payload-Min. Fuel', 'Max. Payload-MTOW','Max. Fuel-
MTOW',...
    'Max Fuel-Min. Flying Weight');
```